action master mix was prepared according to the manufacturer's protocol to give final concentrations of 1× reaction buffer, 300 μM 2′-deoxyadenosine 5′-triphosphate, 300 μM 2′-deoxycytidine 5′-triphosphate, 300 μM 2′-deoxyguanosine 5′-triphosphate, 600 μM 2′-deoxyuridine 5′-triphosphate, 3 mM $Mn(OAc)_2$, 0.1 U/μl *rTth* DNA polymerase, 0.01 U/μl AmpErase UNG, 200 nM AM primers, and 100 nM TaqMan probe. To perform PCR, the RT reaction was incubated at 60°C for 30 min, followed by incubation at 95°C for 5 min to deactivate AmpErase UNG. The present PCR employed was performed using 40 amplification cycles (using 1,000 ng of RNA for *LAT1* mRNA and 50 ng of RNA for *GAPDH* mRNA) at 95°C for 20 s and at 60°C for 1 min. For this, an ABI PRISM 7700 Sequence detector (Applied Biosystems) was used. Total RNA extracts from lung cancer were used as control templates (total RNA: 1,000, 200, 40, and 8 ng for *LAT1* mRNA; 200, 40, 8, and 1.6 ng for *GAPDH* mRNA). Increase in fluorescence was proportional to the concentration of the template in the present PCR (Fig. 2a). Threshold cycle was calculated by determining the point at which the fluorescence exceeded a threshold limit (ten times the standard deviation of the baseline). In other words, signals were regarded as positive if the fluorescence intensity exceeded ten times the standard deviation of the baseline fluorescence. A standard curve was obtained using the threshold cycles established separately for four wells for each applied RNA amount (Fig. 2b). PCR products were separated by electrophoresis in a 3% agarose gel then stained with ethidium bromide (Fig. 2c).

In situ hybridization

In situ hybridization was performed essentially as previously described [16]. Briefly, sections of 35 normal lung tissues, 34 AAH, and 43 NMBAC (measuring 20 mm or less in the greatest diameter) were treated with 0.2 N HCl for 20 min, incubated in 2× standard sodium citrate (SSC) for 10 min at 37°C, and incubated in 5 μg/ml proteinase K for 10 min at 37°C. Sections were subsequently post-fixed in 4% paraformaldehyde for 5 min, then incubated in 0.1 M triethanolamine buffer (pH 8.0) containing 0.25% (vol/vol) acetic anhydride for 10 min to prevent nonspecific binding due to oxidation of the tissue. Hybridization was carried out overnight at 42°C in 50% (vol/vol) deionized formamide, 5× Denhardt's solution, 5% (wt/vol) dextran sulfate, 2× SSC, 0.3 mg/ml salmon sperm DNA, 5 mM ethylenediaminetetraacetic acid, and 10 ng/ml biotin-labeled probes. After performing a final stringent wash at 37°C for 20 min, hybridization was detected immunologically. The *LAT1* cDNA probe used was a 251-bp fragment (obtained from positions 918 to 1,168 in the cDNA of *LAT1*) subcloned into the *Eco*RI site of a pGEM-T Easy Vector (Promega, Madison, WI). Antisense probes and corresponding sense probes were labeled with biotin using SP6 and T7 polymerases, respectively, by means of an RNA labeling kit (Roche Diagnostics, Mannheim, Germany).

Immunohistochemistry

We used polymer peroxidase method (EnVision+/HRP; Dako Cytomation, Denmark) on deparaffinized sections of

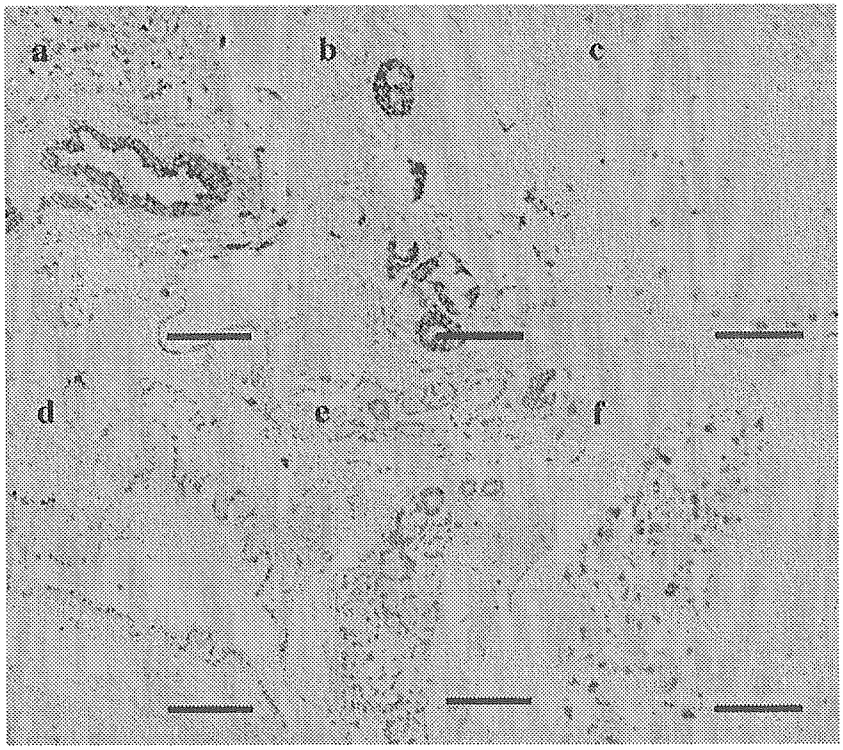

Fig. 1 LAT1 mRNA and protein expressions in normal lung tissues viz. bronchial surface epithelial cells in the bronchus (**a**, **d**), serous cells of the bronchial glands (**b**, **e**), and chondrocytes of the bronchial cartilage (**c**, **f**). *LAT1* mRNA appeared diffuse in the cytoplasm of positive cells within the normal lung. LAT1 protein was expressed as a single nodular spot in the cytoplasm of bronchial surface epithelial cells (**d**), while it was detected as a granular spreading pattern within the cytoplasm of lung components (**e**, **f**), except the bronchial surface epithelial cells. *Scale bar*, 100 μm

Table 1 Expressions of LAT1 mRNA and protein in normal lung

Anatomical site	Number of lesions	*LAT1* mRNA expression [*n* (%)]	LAT1 protein expression [*n* (%)]
Bronchus			
Surface epithelial cells	35	35 (100)	35 (100)
Nonciliated bronchiolar epithelial cells	35	0 (0)	0 (0)
Goblet cells	35	0 (0)	0 (0)
Chondrocytes of the bronchial cartilage	24	22 (91.7)	20 (83.3)
Bronchial glands			
Serous cells	23	15 (65.2)	17 (73.9)
Mucinous cells	23	0 (0)	0 (0)
Alveolar cells			
Type 1 cells	35	0 (0)	0 (0)
Type 2 cells	35	0 (0)	0 (0)
Alveolar macrophages	35	35 (100)	35 (100)

35 normal lung tissues, 34 AAH, and 43 NMBAC (measuring 20 mm or less in the greatest diameter), employing mouse monoclonal antibodies against LAT1 (1:20; clone no. 4D9; Transgenic, Kumamoto, Japan) and Ki-67 (1:20; clone no. Ki-55; Dako Cytomation, Tokyo, Japan). The sections received autoclave pretreatment of 0.05 M citrate buffer (pH 6.0) for 20 min before immunohistochemistry against both antibodies. For negative control, incubation step with the primary antibody was omitted. In absorption tests for LAT1, sections were treated with the primary antibody in the presence of LAT1 peptide.

Data analysis

For in situ hybridization and immunoreactivity analyses, staining was scored as: (−) negative reaction of tumor cells; (±) <10% of tumor area stained; (+) 11–25% stained; (2+) 26–50% stained; or (3+) ≥51% stained. The tumors in which stained tumor cells made up more than 25% of the

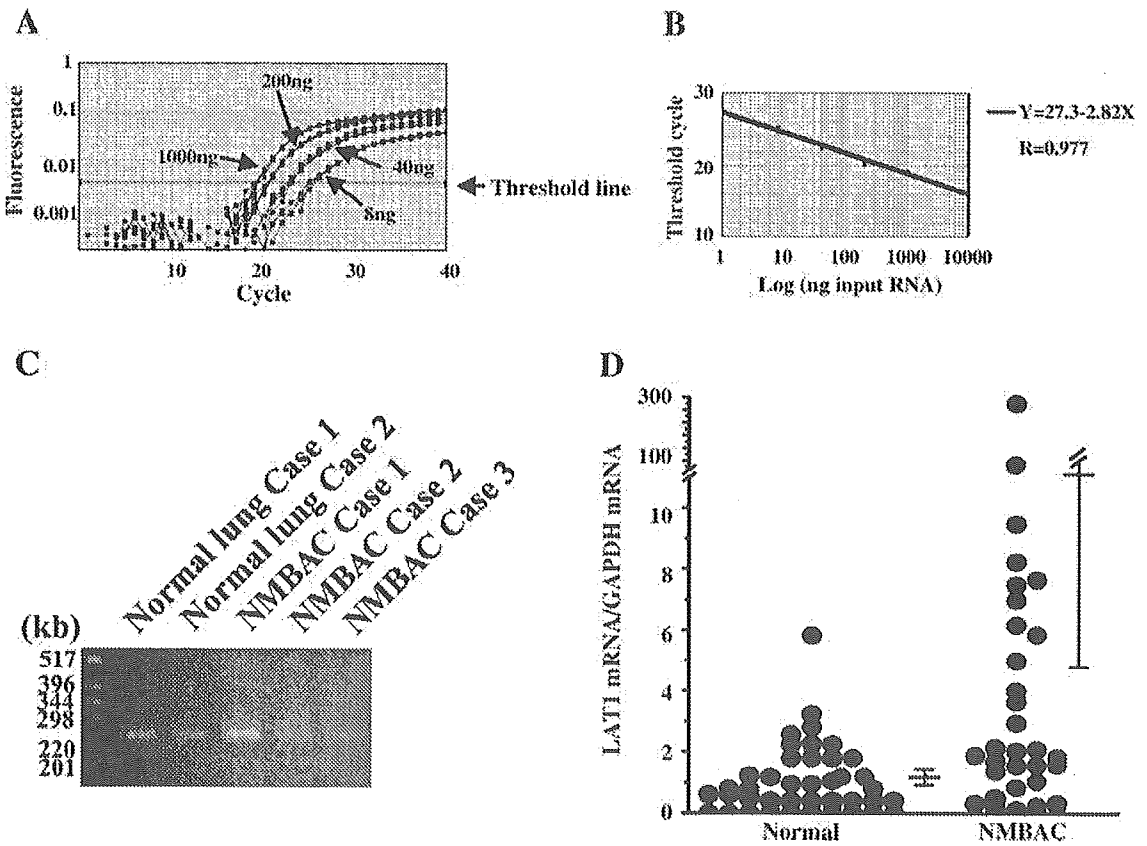

Fig. 2 Semiquantitative RT-PCR for *LAT1* mRNA. **a** Amplification plot obtained in real time using the semiquantitative RT-PCR method. Total RNA (1,000, 200, 40, and 8 ng) extracted from lung cancer was subjected to RT-PCR. **b** Standard curve for the threshold cycle of RT-PCR. The threshold cycle (obtained in quadruplicate) was plotted for each of the four RNA amounts applied. **c** Detection of PCR products. For instance, five PCR products (in two noncancerous normal lung tissues and in tumors from three patients with peripherally located NMBAC) were detected at 251 bp. **d** Levels of *LAT1* mRNA/*GAPDH* mRNA in normal lung tissues (n=41) and NMBAC (n=34). When the actual "*LAT1* mRNA/*GAPDH* mRNA" value obtained for normal lung tissues in one individual patient was expressed as "1.0" and all other values were expressed in a relative manner, the mean ± SEM values obtained for the *LAT1* mRNA/*GAPDH* mRNA levels in 34 NMBAC and 41 normal lung tissues were 12.0±8.1 and 1.0±0.2, respectively. These levels tended to be higher for NMBAC than for normal lung tissues. Furthermore, 9 of 34 NMBAC (26.4%) had values higher than 5.8 (which was the highest value detected in the normal lung tissues)

tumor were graded as positive. For Ki-67 analysis, the percentage of nuclei exhibiting a positive immunoreaction (Ki-67 index) was determined based on immunoreactions in at least 1,000 cells.

Statistical analysis of differences in incidence between two groups was performed using chi-square analysis, while that of differences between two groups in levels of *LAT1* mRNA/*GAPDH* mRNA or the Ki-67 labeling index was performed using unpaired Student's *t* test. A value of $p<0.05$ was considered significant.

Results

Distributions of LAT1 mRNA and protein in normal lung

On in situ hybridization analysis, *LAT1* mRNA appeared diffuse in the cytoplasm of positive cells within the normal lung (Fig. 1). Detection of *LAT1* mRNA was as follows: 100% for bronchial surface epithelial cells (35 of 35 cases), 91.7% for chondrocytes of the bronchial cartilage (22 of 24 cases), 65.2% for serous cells of bronchial glands (15 of 23 cases), and 100% for alveolar macrophages (35 of 35 cases), but it was zero for nonciliated bronchiolar epithelial cells (Clara cells), goblet cells of the bronchus, mucinous cells of the bronchial glands, and alveolar type I or type II cells (Table 1, Fig. 1).

On immunohistochemistry analysis, LAT1 protein appeared granular in the cytoplasm of chondrocytes of the bronchial cartilage, serous cells of the bronchial glands, and alveolar macrophages within the normal lung (Fig. 1). In the cytoplasm of bronchial surface epithelial cells, however, the expression of LAT1 protein appeared as a single nodular spot, described as nodular-type staining, which was considered to represent an intracellularly localized nonfunctional protein. In the absorption test for LAT1 antibody, no LAT1 protein was detected using immunohistochemistry (data not shown). The following findings for LAT1 protein were similar to those described above for *LAT1* mRNA. LAT1 protein detection was as follows: 100% for bronchial surface epithelial cells (35 of 35 cases), 83.3% for chondrocytes of the bronchial cartilage (20 of 24 cases), 73.9% for serous cells of the bronchial glands (17 of 23 cases), and 100% for alveolar macrophages (35 of 35 cases), but it was zero for nonciliated bronchiolar epithelial cells (Clara cells), goblet cells of the bronchus, mucinous cells of the bronchial glands, and alveolar type I or type II cells (Table 1, Fig. 1).

Semiquantitative RT-PCR for *LAT1* mRNA in normal lung tissue and NMBAC

Polymerase chain reaction products were detected at 251 bp in noncancerous normal lung tissues and NMBAC (Fig. 2c). *GAPDH* mRNA levels (obtained using a total RNA of 50 ng for each sample) ranged from 0.72 to 18 ng (as control RNA levels). Therefore, semiquantitative RT-PCR for *LAT1* mRNA was performed using a total RNA of 1,000 ng for each sample. When the actual "*LAT1* mRNA/*GAPDH* mRNA" value obtained for normal lung tissues in one individual patient was expressed as "1.0" and all other values were expressed in a relative manner, the mean ±

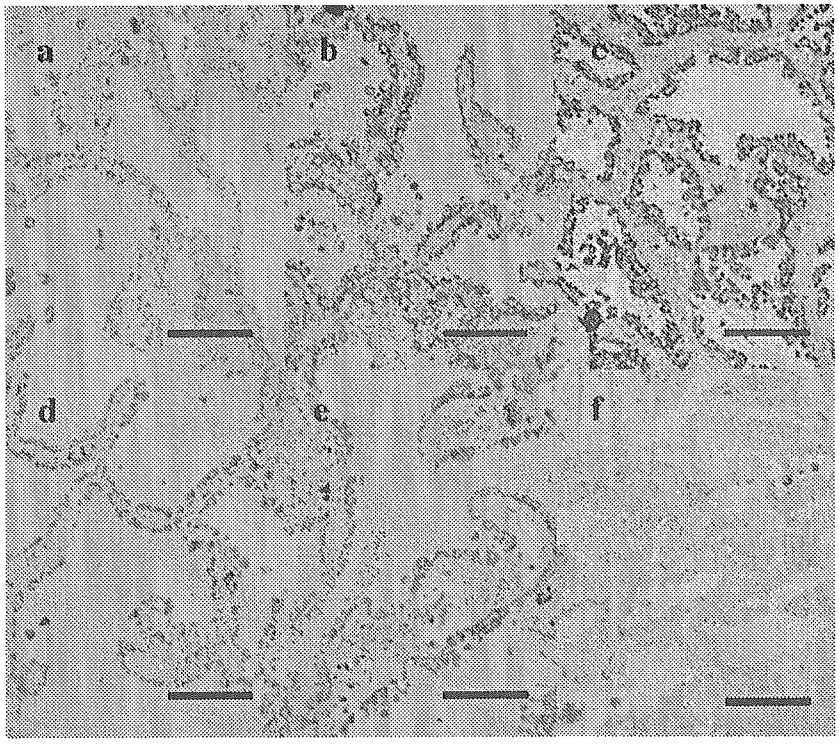

Fig. 3 LAT1 mRNA and protein expressions in low-grade AAH (*positive reaction*; **a**, **d**), high-grade AAH (*positive reaction*; **b**, **e**), and peripherally located NMBAC (*positive reaction*; **c**, **f**). *LAT1* mRNA was localized to within the cytoplasm of cells in AAH and NMBAC by in situ hybridization, whereas LAT1 protein was localized in the plasma membrane as well as the cytoplasm of cells in AAH and NMBAC by immunohistochemistry. *Scale bar*, 100 μm

Table 2 Expressions of LAT1 mRNA and protein in AAH and NMBAC of the lung

Lung condition	Number of lesions	*LAT1* mRNA expression [*n* (%)]	LAT1 protein expression [*n* (%)]
AAH			
Total	34	21 (61.8)	15 (44.1)*
Low grade	11	6 (54.5)	3 (27.3)**
High grade	23	15 (65.2)	12 (52.2)
NMBAC	43	28 (65.1)	34 (79.1)*,**

Statistical analysis was performed using chi-square analysis
*p=0.0015
**p=0.0010

standard error of the mean (SEM) values obtained for the *LAT1* mRNA/*GAPDH* mRNA levels in 34 NMBAC and 41 normal lung tissues were 12.0±8.1 and 1.0±0.2, respectively (Fig. 2d). These levels tended to be higher for NMBAC than for normal lung tissues, although a significant difference between normal lung tissues and NMBAC was not detected (p=0.13). The *LAT1* mRNA/*GAPDH* mRNA levels covered a much wider range (from 0 to 276) in NMBAC than in normal lung tissues (from 0 to 5.8). Moreover, six NMBAC had values higher than 7.0, whereas 5.8 was the highest value detected in the normal lung tissues.

Clinicopathological findings of AAH

There were 19 patients with a total of 34 AAH lesions. Nine of these 19 patients were male. Age at diagnosis was within the range 51–77 years, with a median age of 62 years. Among the 19 cases with 34 AAH lesions, 12 cases showed only one AAH lesion. Four of these 12 cases had only AAH lesions, without lung cancer. Among the 15 cases of lung cancer, there were 13 cases of adenocarcinoma, 1 case of squamous cell carcinoma, and 1 case of large cell carcinoma. Each AAH lesion in a patient with carcinoma was completely separated from the carcinoma by macroscopic examination, and in sections on a slide by microscopic examination. The diameter of the AAH lesions was within the range 1–20 mm, with a median diameter of 5 mm. In terms of diameter, there was no significant difference between low-grade AAH lesions (mean ± SD, 6.1±4.5 mm) and high-grade AAH lesions (mean ± SD, 6.1±3.9 mm). Of the 34 AAH lesions, 23 were interpreted as high-grade based on the findings of increased cellularity and cytological pleomorphism.

Expressions of LAT1 mRNA and protein in AAH and NMBAC

Expression of *LAT1* mRNA was confined to the cytoplasm of hyperplastic and neoplastic cells (Fig. 3). A positive *LAT1* mRNA expression was recognized in 61.8% of all AAH (21 of 34 lesions) [54.5% of low-grade AAH (6 of 11 lesions) and 65.2% of high-grade AAH (15 of 23 lesions)] and in 65.1% of NMBAC (28 of 43 lesions). LAT1 protein was detected in the cytoplasm and on the plasma membrane of hyperplastic and neoplastic cells (Fig. 3). The intensity of LAT1 protein staining sometimes varied within a given case. A positive LAT1 protein expression was recognized in 44.1% of all AAH (15 of 34 lesions) [27.3% of low-grade AAH (3 of 11 lesions) and 52.2% of high-grade AAH (12 of 23 lesions)] and in 79.1% of NMBAC (34 of 43 lesions). In the seven cases with multiple AAH (four cases with two AAH, two cases with four AAH, and one case with six AAH), the intensity and immunoreactive area varied among the multiple AAH in each case. The incidence of a positive expression for LAT1 protein was significantly different between total AAH and NMBAC, and between low-grade AAH and NMBAC (p=0.0015 and p=0.0010, respectively; Table 2).

Relationship between Ki-67 index and incidences of LAT1 mRNA and protein in AAH and NMBAC

The Ki-67 labeling index (taken as a cell proliferation score) increased from low-grade AAH (mean ± SEM, 1.6± 0.3, ten lesions) to high-grade AAH (3.0±0.6, nine lesions) to NMBAC (7.4±0.7, 33 tumors). Significant differences were detected between total AAH and NMBAC, between low-grade AAH and NMBAC, and between high-grade AAH and NMBAC (p<0.0001, p<0.0001, and p=0.0062, respectively). The Ki-67 labeling index was significantly higher in those AAH and NMBAC that were positive for LAT1 protein than their LAT1-protein-negative counterparts (p=0.037 and p=0.034, respectively; Table 3).

Table 3 Ki-67 labeling index in AAH and NMBAC of the lung

Lung condition	Number of lesions	*LAT1* mRNA		LAT1 protein	
		Positive	Negative	Positive	Negative
AAH					
Total	19	2.7±0.4[a] (12)	1.5±0.4 (7)	3.2±0.6 (7)*	1.7±0.3 (12)*
Low grade	10	2.0±0.3 (6)	1.1±0.4 (4)	2.2±0.6 (3)	1.4±0.3 (7)
High grade	9	3.6±0.7 (6)	2.0±0.6 (3)	3.9±1.0 (4)	2.3±0.6 (5)
NMBAC	33	7.2±0.8 (22)	8.0±1.6 (11)	8.3±0.8 (25)**	4.7±0.9 (8)**

Statistical analysis was performed using an unpaired Student's t test
[a]Mean±SEM (number of cases)
*p=0.037
**p=0.034

Discussion

In the present study, we measured the levels of *LAT1* mRNA/*GAPDH* mRNA in normal lung tissues and NMBAC measuring 30 mm or less in the greatest diameter, and then applied in situ hybridization and immunohistochemistry to the normal lung, AAH, and NMBAC measuring less than 20 mm in diameter. Although the levels of *LAT1* mRNA/*GAPDH* mRNA failed to show a significant difference between normal lung tissues and NMBAC using semiquantitative RT-PCR, we observed that the incidence of a positive expression for LAT1 protein increased or tended to increase from low-grade AAH to high-grade AAH to NMBAC (with the incidence in high-grade AAH apparently being intermediate between those in low-grade AAH and NMBAC and tending to be closer to the latter than to the former). Furthermore, the Ki-67 labeling index (a cell proliferation score) was significantly higher in LTA1-protein-positive AAH and NMBAC than in their LAT1-protein-negative counterparts. Hence, our results are consistent with an upregulation of metabolic activity in both high-grade AAH and NMBAC alongside an upregulation of LAT1 protein.

It has previously been reported that LAT1 is expressed in some normal tissues, including the blood–brain barrier, activated lymphocytes, basal layer of the skin, proximal tubules of the kidney, placenta, and testis, and also in a variety of tumor cells such as glioma, breast cancer, bladder cancer, and colon cancer [8, 11, 19, 21, 23, 26]. To our knowledge, however, LAT1 expression has not previously been reported in the normal lung. We observed, using in situ hybridization and immunohistochemistry, that LAT1 mRNA and protein were expressed in a variety of lung components (including bronchial surface epithelial cells, serous cells of the bronchial glands, alveolar macrophages, and chondrocytes of the bronchial cartilage), although they were not detected in nonciliated bronchiolar epithelial cells (Clara cells), type I alveolar epithelial cells, type II alveolar epithelial cells, or mucinous cells of the bronchial glands. It should be noted that LAT1 protein in the bronchial surface epithelial cells was localized only to the cytoplasm, with a nodular pattern appearance that was considered to be nonfunctional (because it was not present on the plasma membrane). By semiquantitative RT-PCR, *LAT1* mRNA/*GAPDH* mRNA levels could be measured in 37 of 41 normal lung tissues, supporting the above results that were obtained using in situ hybridization and immunohistochemistry. Furthermore, the *LAT1* mRNA/*GAPDH* mRNA levels observed in normal lung tissues covered quite a wide range (from 0 to 5.8). This variety of levels may be due to heterogeneity or disproportionality among lung cell components.

In the present study, the *LAT1* mRNA/*GAPDH* mRNA values covered a much wider range (from 0 to 276) in NMBAC than in normal lung tissues (see above). In particular, six NMBAC (17.6%) had values higher than 7.0, and nine NMBAC (26.4%) had values higher than 5.8, which was the highest value obtained for the normal lung. Moreover, the mean NMBAC value tended to be higher than that obtained for normal lung tissues. Furthermore, *LAT1* mRNA was not detected in Clara cells or in type II alveolar epithelial cells in normal lung specimens using in situ hybridization. Based on these findings, the mean *LAT1* mRNA/*GAPDH* mRNA value may be lower in normal peripheral lung tissues (if we exclude cell components comprising central lung tissues, such as bronchial surface epithelial cells, serous cells of the bronchial glands, and chondrocytes of the bronchial cartilage) than in NMBAC. Furthermore, our immunohistochemical results indicate that bronchial surface epithelial cells in the central bronchi and peripheral bronchioles may produce a nonfunctional LAT1 protein (judging from the nodular-type cytoplasmic staining pattern), whereas the LAT1 protein is detected in the plasma membrane as well as in the cytoplasm in NMBAC. Thus, functional LAT1 protein may be produced at significantly higher levels in NMBAC than in normal lung tissues.

It is generally accepted that NMBAC was derived from nonbronchiolar epithelial cells (Clara cells) or type II alveolar epithelial cells, based on the phenotypic expression of neoplastic cells [9, 12]. In our in situ hybridization and immunohistochemical investigations, *LAT1* mRNA and protein were not detected in Clara cells or in type II alveolar epithelial cells in normal lung specimens. Campbell and Thompson [1], who transiently overexpressed LAT1 and 4F2hc (either alone or together) in nontransformed mouse hepatocytes, demonstrated that overexpression of LAT1 alone was sufficient to significantly increase system L transport activity in these hepatocytes, and that hepatic cells overexpressing LAT1 displayed a growth advantage relative to control cells under conditions involving limited arginine. Therefore, they suggested that LAT1 overexpression was an early event in hepatocarcinogenesis and that it provided neoplastic cells with selective growth or survival advantage, particularly under conditions of nutrient stress. Sang et al. [21] noted that TA1/E16, a partial sequence corresponding to LAT1, was expressed in rat-transformed cell lines and rat fetal liver, but not in adult liver. This led Campbell and Thompson [1] to propose that cells in which LAT1 was not normally expressed, such as hepatocytes, may acquire a growth advantage if LAT1 became constitutively expressed at some stage. This idea would support its involvement in the tumor growth of a lung adenocarcinoma if NMBAC acquired the ability to produce LAT1 during cancer development, although the induction of LAT1 expression may be an effect related to the upregulation of metabolic activity in AAH and NMBAC.

In the results obtained by in situ hybridization, the incidence of *LAT1* mRNA expression was relatively high (between 54.5 and 65.2%) in AAH and NMBAC, and no difference in the incidence of *LAT1* mRNA expression was detected between AAH and NMBAC. In contrast, the incidence of LAT1 protein expression increased or tended to increase from low-grade AAH to high-grade AAH to NMBAC, and a significant difference in its incidence was found between total AAH and NMBAC. The reason for this discrepancy between the incidence of *LAT1* mRNA (already high in low-grade AAH) and that of LAT1 protein

(progressive increase from low-grade AAH to high-grade AAH to NMBAC) is unclear. One possibility is that a rapid increase in *LAT1* mRNA may occur at the very early stage in the development of a lung carcinoma, with the subsequent synthesis of LAT1 protein occurring slowly throughout the development of this carcinoma. Another possibility is that, for reasons as yet unknown, LAT1 protein might be broken down more rapidly in the early stages of this development than in the later stages. Be that as it may, it would appear that *LAT1* mRNA expression may be a useful marker for evaluating early events in the pathogenesis of NMBAC. Furthermore, our results reveal a discrepancy between the incidence of *LAT1* mRNA (65.1%) and that of LAT1 protein (79.1%) in NMBAC. Although the reason for this discrepancy is as yet unclear, one possibility is that the probe used for in situ hybridization may be of lower sensitivity than the antibody used for immunohistochemistry. In addition, we reveal heterogeneities in expressions of LAT1 protein and mRNA among multiple AAH in individual cases, suggesting that AAH may be heterogeneous in terms of metabolic activity, cell growth, and the potential to progress to NMBAC. However, a limitation of this study was that we had only a small number (two cases) of NMBAC materials measuring 20 mm or less in the greatest diameter for RT-PCR, and no AAH. Moreover, the number of low-grade AAH lesions was lower than the number of high-grade AAH and NM BAC lesions. Confirmation of a role for LAT1 in AAH and NMBAC would need evidence from a large-scale study using molecular techniques.

In the present study, the Ki-67 labeling index increased from low-grade AAH to high-grade AAH to NMBAC, indicating a gain in proliferative activity from premalignant cells to malignant cells. These results are similar to findings described previously [9]. Furthermore, the Ki-67 labeling index was significantly higher in LTA1-protein-positive AAH and NMBAC than in their LAT1-protein-negative counterparts. These results suggest that the proliferating cells in AAH and NMBAC underwent an increase in their metabolism, with an associated upregulation of LAT1 protein.

In conclusion, the results of our study on LAT1 are consistent with high-grade AAH being a lesion closely associated with NMBAC of the lung. Furthermore, LAT1 protein overexpression in AAH and NMBAC shows a significant association with the Ki-67 labeling index, indicating an upregulation of metabolic activity. Finally, it is well-known that LAT1 requires 4F2hc for its functional expression. Furthermore, 4F2hc has been reported to induce cell proliferation and to be expressed in numerous tissues [20]. In the present study, we could not investigate the possible link between the functional role of 4F2hc and the overexpression of LAT1 (because a suitable 4F2hc antibody was not available to us). Therefore, further investigations of AAH, on a larger scale, will be necessary to establish whether 4F2hc expression at the plasma membrane correlates with metabolic activity and cell growth in AAH and NMBAC.

Acknowledgements We thank Dr. Robert Timms for correcting the English version of the manuscript. The anti-LAT1 antibody was supplied by Kumamoto Immunochemical Laboratory, Transgenic.

References

1. Campbell WA, Thompson NL (2001) Overexpression of LAT1/CD98 light chain is sufficient to increase system L-amino acid transport activity in mouse hepatocytes but not fibroblasts. J Biol Chem 276:16877–16884
2. Christensen HN (1990) Role of amino acid transport and countertransport in nutrition and metabolism. Physiol Rev 70:43–77
3. Chillaron J, Roca R, Valencia A, Zorzano A, Palacin M (2001) Heteromeric amino acid transporters: biochemistry, genetics, and physiology. Am J Physiol Renal Physiol 281:F995–F1018
4. Chomczyski P, Sacchi N (1987) Single-step method of RNA isolation by acid guanidium thiocyanate–phenol–chloroform extraction. Anal Biochem 162:156–159
5. Kanai Y, Endou H (2003) Functional properties of multispecific amino acid transporters and their implications to transporter-mediated toxicity. J Toxicol Sci 28:1–17
6. Kanai Y, Endou H (2001) Heterodimeric amino acid transporters: molecular biology and pathological and pharmacological relevance. Curr Drug Metab 2:339–354
7. Kanai Y, Segawa H, Miyamoto K, Uchino H, Takeda E, Endou H (1998) Expression cloning and characterization of a transporter for large neutral amino acids activated by the heavy chain of 4F2 antigen (CD98). J Biol Chem 273:23629–23632
8. Kim DK, Kanai Y, Choi HW, Tangtrongsup S, Chairoungdua A, Babu E, Tachampa K, Anzai N, Iribe Y, Endou H (2002) Characterization of the system L amino acid transporter in T24 human bladder carcinoma cells. Biochim Biophys Acta 1565: 112–121
9. Kitamura H, Kameda Y, Ito T, Hayashi H (1999) Atypical adenomatous hyperplasia of the lung. Am J Clin Pathol 111: 610–622
10. Mastroberardino L, Spindler B, Pfeiffer R, Skelly PJ, Loffing J, Shoemaker CB, Verrey F (1998) Amino-acid transport by heterodimers of 4F2hc/CD98 and members of a permease family. Nature 395:288–291
11. Matsuo H, Tsukada S, Nakata T, Chairoungdua A, Kim DK, Cha SH, Inatomi J, Yorifuji H, Fukuda J, Endou H, Kanai Y (2000) Expression of a system L neutral amino acid transporter at the blood–brain barrier. NeuroReport 11:3507–3511
12. Mori M, Rao SK, Popper HH, Cagle PT, Fraire AE (2001) Atypical adenomatous hyperplasia of the lung: a possible forerunner in the development of adenocarcinoma of the lung. Mod Pathol 14:72–84
13. Nakanishi K (1990) Alveolar epithelial hyperplasia and adenocarcinoma of the lung. Arch Pathol Lab Med 114:363–368
14. Nakanishi K, Kawai T, Kumaki F, Hiroi S, Mukai M, Ikeda E (2002) Expression of human telomerase RNA component (hTERC) and telomerase reverse transcriptase (hTERT) mRNA in atypical adenomatous hyperplasia of the lung. Hum Pathol 33:697–702
15. Nakanishi K, Kawai T, Kumaki F, Hiroi S, Mukai M, Ikeda E (2003) Survivin expression in atypical adenomatous hyperplasia of the lung. Am J Clin Pathol 120:712–719
16. Nakanishi K, Kawai T, Kumaki F, Hiroi S, Mukai M, Ikeda E, Koering CE, Gilson E (2003) Expression of mRNAs for telomeric repeat binding factor (TRF)-1 and TRF2 in atypical adenomatous hyperplasia and adenocarcinoma of the lung. Clin Cancer Res 9:1105–1111

17. Nakanishi K, Hiroi S, Kawai T, Suzuki M, Torikata C (1998) Argyrophilic nucleolar-organizer region counts and DNA status in bronchioloalveolar epithelial hyperplasia and adenocarcinoma of the lung. Hum Pathol 29:235–239
18. Nakanishi K, Uenoyama M, Tomita N, Morishita R, Kaneda Y, Ogihara T, Matsumoto K, Nakamura T, Maruta A, Matsuyama S, Kawai T, Aurues T, Hayashi T, Ikeda T (2002) Gene transfer of human hepatocyte growth factor into rat skin wounds mediated by liposomes coated with the sendai virus (hemagglutinating virus of Japan). Am J Pathol 161:1761–1772
19. Ohkame H, Masuda H, Ishii Y, Kanai Y (2001) Expression of L-type amino acid transporter 1 (LAT1) and 4F2 heavy chain (4F2hc) in liver tumor lesions of rat models. J Surg Oncol 78:265–271
20. Parmacek MS, Karpinski BA, Gottesdiener KM, Thompson CB, Leiden JM (1989) Structure, expression and regulation of the murine 4F2 heavy chain. Nucleic Acids Res 17:1915–1931
21. Sang J, Lim YP, Panzica M, Finch P, Thompson NL (1995) TA1, a highly conserved oncofetal complementary DNA from rat hepatoma, encodes an integral membrane protein associated with liver development, carcinogenesis, and cell activation. Cancer Res 55:1152–1159
22. Segawa H, Fukasawa Y, Miyamoto K, Takeda E, Endou H, Kanai Y (1999) Identification and functional characterization of a Na^+-independent neutral amino acid transporter with broad substrate selectivity. J Biol Chem 274:19745–19751
23. Shennan DB, Thomson J, Barber MC, Travers MT (2003) Functional and molecular characteristics of system L in human breast cancer cells. Biochim Biophys Acta 1611:81–90
24. Shimosato Y, Kodama T, Kameya T (1982) Morphogenesis of peripheral type adenocarcinoma of the lungs. In: Shimosato Y, Melamed MR, Nettesheim P (eds) Morphogenesis of lung cancer, vol 1. CRC Press, Boca Raton, FL, pp 65–89
25. Travis, WD, Colby TV, Corrin B, Shimosato T, Brambilla E (1999) World Health Organization international histologic classification of tumours. Histological typing of lung and pleural tumours, 3rd edn. Springer, Berlin Heidelberg New York, p 36
26. Wolf DA, Wang S, Panzica MA, Bassily NH, Thompson NL (1996) Expression of a highly conserved oncofetal gene, TA1/E16, in human colon carcinoma and other primary cancers: homology to *Schistosoma mansoni* amino acid permease and *Caenorhabditis elegans* gene products. Cancer Res 56:5012–5022

Dual-Color Imaging of Nuclear-Cytoplasmic Dynamics, Viability, and Proliferation of Cancer Cells in the Portal Vein Area

Kazuhiko Tsuji,[1,2,3] Kensuke Yamauchi,[1] Meng Yang,[1] Ping Jiang,[1] Michael Bouvet,[2] Hitoshi Endo,[3] Yoshikatsu Kanai,[3] Koji Yamashita,[1] Abdool R. Moossa,[2] and Robert M. Hoffman[1,2]

[1]AntiCancer, Inc.; [2]Department of Surgery, University of California, San Diego, California; and [3]Department of Pharmacology and Toxicology, Kyorin University, Tokyo, Japan

Abstract

We used dual-color *in vivo* cellular imaging to visualize trafficking, nuclear-cytoplasmic dynamics, and the viability of cancer cells after their injection into the portal vein of mice. For these studies, we used dual-color fluorescent cancer cells that express green fluorescent protein (GFP) linked to histone H2B in the nucleus and retroviral red fluorescent protein (RFP) in the cytoplasm. Human HCT-116-GFP-RFP colon cancer and mouse mammary tumor (MMT) cells were HCT-116-GFP-RFP in the portal vein of nude mice. The cells were observed intravitally in the liver at the single-cell level using the Olympus OV100 whole-mouse imaging system. Most HCT-116-GFP-RFP cells remained in sinusoids near peripheral portal veins. Only a small fraction of the cancer cells invaded the lobular area. Extensive clasmocytosis (destruction of the cytoplasm) of the HCT-116-GFP-RFP cells occurred within 6 hours. The number of apoptotic cells rapidly increased within the portal vein within 12 hours of injection. Apoptosis was readily visualized in the dual-color cells by their altered nuclear morphology. The data suggest rapid death of HCT-116-GFP-RFP cells in the portal vein. In contrast, dual-color MMT-GFP-RFP cells injected into the portal vein mostly survived in the liver of nude mice 24 hours after injection. Many surviving MMT-GFP-RFP cells showed invasive figures with cytoplasmic protrusions. The cells grew aggressively and formed colonies in the liver. However, when the host mice were pretreated with cyclophosphamide, the HCT-116-GFP-RFP cells also survived and formed colonies in the liver after portal vein injection. These results suggest that a cyclophosphamide-sensitive host cellular system attacked the HCT-116-GFP-RFP cells but could not effectively kill the MMT-GFP-RFP cells. (Cancer Res 2006; 66(1): 303-6)

Introduction

The portal vein is a critical route for cancer cell metastasis to the liver. However, the early fate of cancer cells in the portal vein circulation is poorly understood because it has been difficult to visualize the behavior of single cancer cells and micrometastasis. Previously, cancer cells were transfected with the *Escherichia coli* β-galactosidase (*lacZ*) gene, which enables detection of micrometastases in tissue sections. However, *lacZ* does not allow direct visualization of cancer cells in live animals (1–5). We developed an approach to visualizing cancer cells *in vivo* through the use of green fluorescent protein (GFP; refs. 1–4).

Requests for reprints: Robert M. Hoffman, AntiCancer, Inc., 7917 Ostrow Street, San Diego, CA 92111. Phone: 858-654-2555; Fax: 858-268-4175; E-mail: all@anticancer.com.

doi:10.1158/0008-5472.CAN-05-2958

Two processes have been proposed to explain the high incidence of colon cancer metastasis in liver. One explanation is based on the seed-and-soil theory of Paget, in which preferential growth of colon cancer cells to the liver forms the basis. Other studies have shown that cancer cells remain in the liver because they are arrested physically in the too-narrow sinusoids of the liver.

Mook et al. (6) used intravital videomicroscopy to visualize early events after injection of GFP-expressing colon cancer cells in the portal vein. Initial arrest of the colon cancer cells in sinusoids of the liver was due to size restriction. Adhesion of cancer cells to endothelial cells was never found. Instead, endothelial cells retracted rapidly and interactions were observed only between cancer cells and hepatocytes. Tumor cells divided exclusively intravascularly during the first 4 days.

Wang et al. (7) also visualized the trafficking of GFP-expressing metastatic cancer cells targeting the liver via the portal vein. Within 72 hours after transplantation of tumor cells on the ascending colon in nude mice, metastasis was visualized *ex vivo* on a single-cell basis around the portal vein by GFP imaging. At this early time point, a few cells were visualized trafficking to the liver via the portal vein. By post-implantation day 5, the caudate lobe of the liver was involved with trafficking metastatic cells, which subsequently formed colonies.

Real-time intravital videomicroscopy analysis of liver metastases after intraportal injection of GFP-expressing cells via a mesenteric vein revealed that both metastatic LM-EGFP and nonmetastatic E2-EGFP rat tongue tumor cells arrested similarly in sinusoidal vessels near terminal portal venules (8). The nonmetastatic E2-EGFP cells were completely eliminated from the liver sinusoids within 3 days, with no solitary dormant cells. However, a substantial number of LM-EGFP cells remained in the liver, possibly due to stable attachment to the sinusoidal wall. The LM-EGFP cells began to grow 3 to 4 days after inoculation (8).

In the current study, we visualized the early trafficking of dual-colored cancer cells, labeled with GFP in the nucleus and red fluorescent protein (RFP) in the cytoplasm (9), injected into the portal vein of nude mice. We report here the fate of different cancer cell types in the portal circulation. We also report the effect of cyclophosphamide pretreatment of the host mouse on the fate of the cancer cells in the portal circulation.

Materials and Methods

Production of RFP retroviral vector. For RFP retrovirus production, the *Hind*III/*Not*I fragment from pDsRed2 (Clontech Laboratories, Inc., Palo Alto, CA), containing the full-length RFP cDNA, was inserted into the *Hind*III/*Not*I site of pLNCX2 (Clontech Laboratories) containing the neomycin resistance gene (4). PT67, an NIH3T3-derived packaging cell line (Clontech Laboratories) expressing the 10 Al viral envelope, was cultured in DMEM (Irvine Scientific, Santa Ana, CA) supplemented with 10% heat-inactivated fetal bovine serum (Gemini Bio-Products, Calabasas, CA).

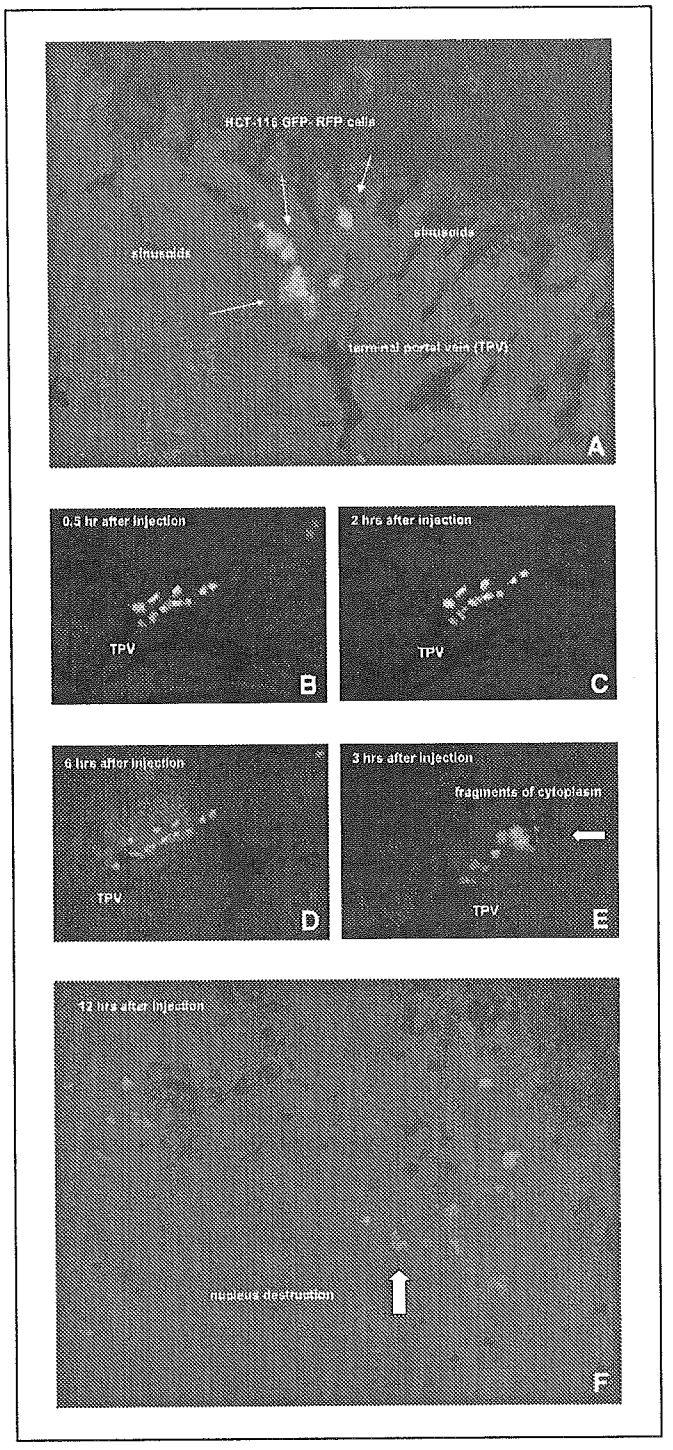

Figure 1. *A-F*, fate of HCT-116-GFP-RFP human colon cancer cells after portal vein injection. A laparotomy was done on nude mice under ketamine anesthesia in order to inject HCT-116 GFP-RFP human colon cancer cells (0.25×10^6) into the portal vein. The nuclei of the cancer cells express GFP linked to histone H2B and the cytoplasm expresses retroviral RFP. The liver was immobilized on a slide glass in order to limit movement. The liver surface was then imaged for dual-color fluorescence in the Olympus OV100 whole-mouse imaging system. The abdomen was opened and then closed for each imaging time point. Time course imaging after injection of HCT-118 RFP-GFP cells is described in (*A-F*). Destruction of RFP-expressing cytoplasm of the cancer cells began rapidly. The destruction of RFP-cytoplasm progressed with time. The stripped nuclei seemed to remain intact within 6 hours after injection. The number of apoptotic cells with fragmented nuclei in the liver increased within 12 hours. Fragmentation of GFP nuclei is clearly seen. In *A*, groups of cells are visible. Individual cells can be visualized in *B-F*.

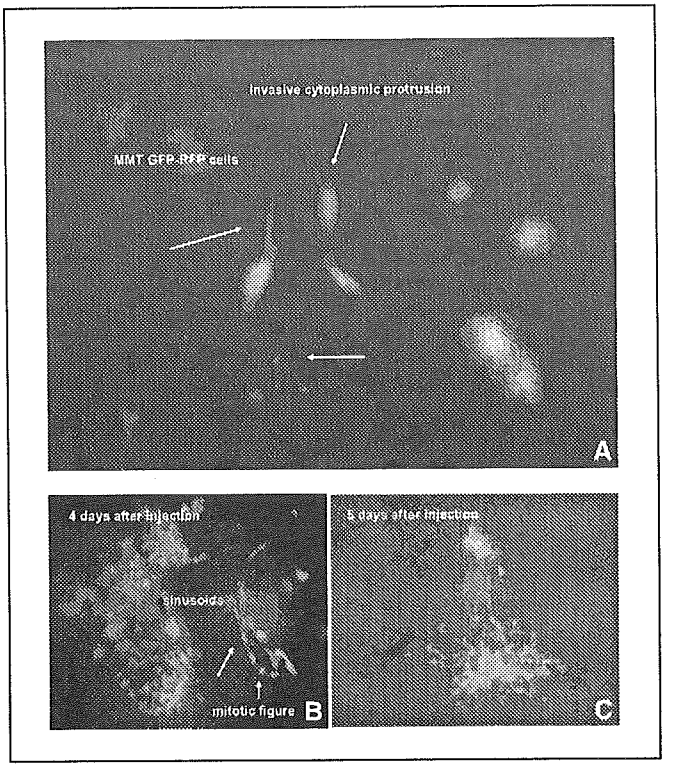

Figure 2. Fate of MMT GFP-RFP mouse mammary tumor cells after portal vein injection. *A*, MMT GFP-RFP mouse mammary tumor cells (0.25×10^6) were injected into the portal vein and imaged as described in Materials and Methods. Most MMT-GFP-RFP cells maintained normal cell structure and survived >24 hours after injection. Some MMT-GFP-RFP cells produced cytoplasmic protrusions which seemed invasive. *B* and *C*, the time course behavior of MMT GFP-RFP cells was imaged after portal vein injection using the methods described above. Many MMT GFP-RFP cells, which impacted into sinusoids near the terminal portal vein after injection, survived and grew into colonies.

For vector production, PT67 cells, at 70% confluence, were incubated with a precipitated mixture of LipofectAMINE reagent (Life Technologies, Inc., Grand Island, NY) and saturating amounts of pLNCX2-DsRed2 plasmid for 18 hours. Fresh medium was replenished at this time. The cells were examined by fluorescence microscopy 48 hours posttransduction. For selection of a clone producing high amounts of RFP retroviral vector (PT67-DsRed2), the cells were cultured in the presence of 200 to 1,000 μg/mL of G418 (Life Technologies) for 7 days. The isolated clone was termed PT67-DSRed2.

Production of histone H2B-GFP vector. The histone H2B gene has no stop codon (10), thereby enabling the ligation of the H2B gene to the 5′-coding region of the GFP gene (Clontech Laboratories; ref. 4). The histone H2B-GFP fusion gene was then inserted at the *Hind*III/*Cal*I site of the pLHCX (Clontech Laboratories), which has the hygromycin resistance gene. To establish a packaging cell clone producing high amounts of histone H2B-GFP retroviral vector, the pLHCX histone H2B-GFP plasmid was transfected in PT67 cells using the same methods described above for PT67-DsRed2. The transfected cells were cultured in the presence of 200 to 400 μg/mL hygromycin (Life Technologies) for 15 days to establish stable PT67 H2B-GFP packaging cells.

RFP and histone H2B-GFP gene transduction of cancer cells. For RFP and H2B-GFP gene transduction, 70% confluent human cancer cells were used (4). To establish dual-color cells, clones expressing RFP in the cytoplasm were initially established. In brief, cancer cells were incubated with a 1:1 precipitated mixture of retroviral supernatants of PT67-RFP cells and RPMI 1640 (Irvine Scientific) containing 10% fetal bovine serum for 72 hours. Fresh medium was replenished at this time. Cells were harvested with trypsin/EDTA 72 hours posttransduction and subcultured at a ratio of

1:15 into selective medium, which contained 200 μg/mL G418. The level of G418 was increased stepwise up to 800 μg/mL. RFP-expressing cancer cells were isolated with cloning cylinders (Bel-Art Products, Pequannock, NJ) using trypsin/EDTA and amplified by conventional culture methods.

For establishing dual-color cancer cells, the cells were then incubated with a 1:1 precipitated mixture of retroviral supernatants of PT67 H2B-GFP cells and culture medium. To select the double transformants, cells were incubated with hygromycin 72 hours after transfection. The level of hygromycin was increased stepwise up to 400 μg/mL.

Animals. Male athymic CD-1 nude mice, between 5 and 6 weeks of age, were used in this study. The animals were bred and maintained in a HEPA-filtered environment with cages, food, and bedding sterilized by autoclaving. The breeding pairs were obtained from Charles River Laboratories (Wilmington, MA). The animal diets were obtained from Harlan Teklad (Madison, WI). Ampicillin 5.0% (w/v; Sigma, St. Louis, MO) was added to the autoclaved drinking water. All animal studies were conducted in accordance with the principles and procedures outlined in the NIH Guide for the Care and Use of Laboratory Animals under assurance no. A3873-1.

Injection of cells: portal vein. The nude mice were anesthetized with a ketamine mixture (10 μL ketamine HCl, 7.6 μL xylazine, 2.4 μL acepromazine maleate, 10 μL H_2O) injected into the peritoneal cavity. Human HCT-116-GFP-RFP colon cancer cells and mouse mammary tumor (MMT)-GFP-RFP cells (0.125-1.0 × 10^6 cells/50 μL) were injected in the portal vein of nude mice during open laparotomy.

Pretreatment of animals with cyclophosphamide. In some experiments, the host mice were pretreated by portal vein injection with cyclophosphamide (100 mg/kg) 6 days and 1 day before injection of HCT-116-GFP-RFP cells into the portal vein.

Visualization of cell trafficking in liver of living mice. At laparotomy, a glass slide was put on the exteriorized liver of the mice to regulate motion. The mice were observed with an Olympus OV100 whole-mouse imaging system. The images were taken immediately after cell injection, and 0.5, 1, 6, 12, and 24 hours, and daily thereafter.

Results and Discussion

Entry of HCT-116-GFP-RFP cells in the portal vein circulation. After the HCT-116-GFP-RFP human colon cancer cells were injected into the main portal vein, cells accumulated in the terminal portal veins. Initially, many HCT-116-GFP-RFP cells

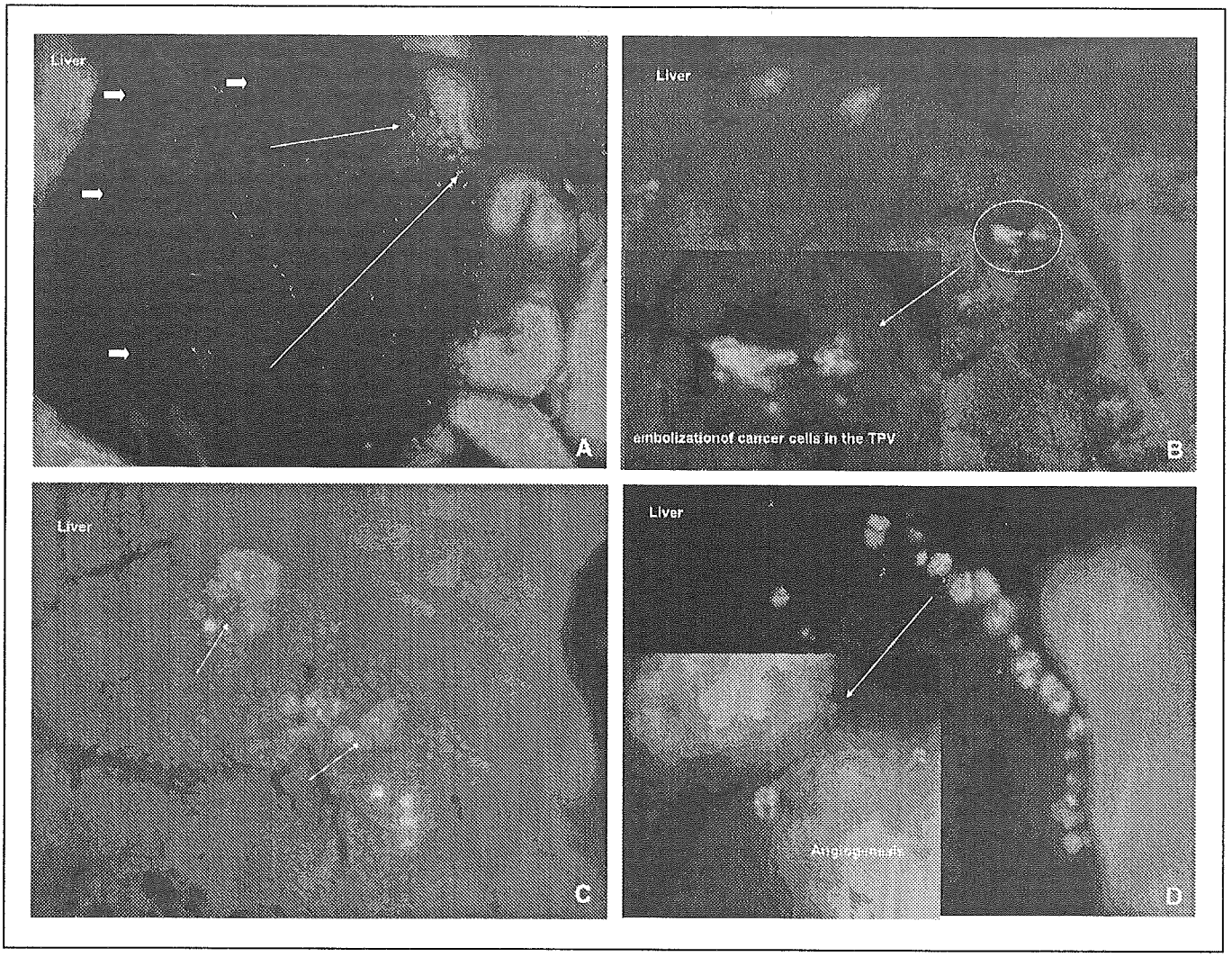

Figure 3. The fate of HCT116 GFP-RFP human colon cancer cells after portal vein injection of cyclophosphamide-pretreated mice. *A*, cyclophosphamide at 100 mg/kg was injected into the portal vein of nude mice on days 1 and 7 before cell injection. HCT116 GFP-RFP cells (1.0 × 10^6) were injected into the portal vein of the cyclophosphamide-pretreated mice. The livers of the mice were intravitally imaged as described above 24 hours later. Many live HCT-116 GFP-RFP cells in the liver were observed. *B*, HCT-116-GFP-RFP cells observed 3 days after injection into cyclophosphamide-pretreated mice. Some injected cancer cells survived and stayed in the terminal portal vein. *C*, colonies of HCT-116-GFP-RFP cells imaged at day 7. *D*, large colonies HCT-116-RFP-GFP cells imaged at day 14.

impacted into sinusoids just after injection (Fig. 1*A*). The diameter size of the sinusoids was ~5 μm. Most HCT-116-GFP-RFP cells remained in the sinusoids near the terminal portal vein.

Time course of HCT-116-GFP-RFP cell death in the portal vein area. Thirty minutes after injection of HCT116-GFP-RFP in the portal vein, 70% of the cells were viable (Fig. 1*B*). However, by 2 hours (Fig. 1*C*), only 50% of the cells were viable, and by 6 hours, only 10% of the cells were viable (Fig. 1*D*). Viability was readily observed as the dead cells were stripped of their RFP-expressing cytoplasm leaving only the GFP nucleus (Fig. 1*E*). The number of apoptotic cells rapidly increased within the portal vein within 12 hours of injection. Fragmentation of GFP nuclei could be clearly visualized (Fig. 1*F*).

Fate of MMT-GFP-RFP cells in the portal vein. MMT-GFP-RFP mouse mammary tumor cells injected into the portal vein had a very different fate in the liver compared with HCT-116-GFP-RFP cells. Although there was rapid cell destruction of some MMT-GFP-RFP cells similar to HCT-116-GFP-RFP cells, many MMT-GFP-RFP cells survived to 24 hours and beyond after injection. Many MMT cells became invasive with cytoplasmic protrusion within 48 hours after injection (Fig. 2). MMT-GFP-RFP cells subsequently formed micrometastasis in the liver from days 2 to 5 (Fig. 2).

Efficacy of cyclophosphamide pretreatment on portal vein viability of HCT-116-GFP-RFP cells. When the host mice were pretreated with cyclophosphamide, the HCT-116-GFP-RFP cells also survived and formed colonies in the liver after portal vein injection, in striking contrast to their rapid cell death in the untreated animals (Fig. 3). These results suggest that a host cellular system attacked the HCT-116-GFP-RFP cells. Most HCT116-GFP-RFP cells survived 24 hours after injection in the cyclophosphamide-treated mice and subsequently formed metastasis in the liver (Fig. 3) in three of five mice compared with none of the non–cyclophosphamide-treated mice. Some of the HCT116-GFP-RFP micrometastases became vascularized by day 14 (Fig. 3).

Morris et al. (8) previously described clasmatosis of cells in the liver. We could visualize this phenomenon more clearly by using bright dual-color fluorescent cancer cells with the cytoplasm labeled with RFP and the nucleus labeled with GFP. HCT-116-GFP-RFP cells injected into the portal vein were all dead within 12 hours. Rapid cell death was also reported by Morris et al. (8). The liver may contain an innate rapid local defense for cells entering the liver portal veins. Our results suggest that such a host defense is sensitive to cyclophosphamide. However, MMT-GFP-RFP cells had a very different fate compared with HCT-116-GFP-RFP cells. The MMT-GFP-RFP cells survived and formed metastases in the liver of untreated nude mice.

The fate of injected malignant cells in the portal vein seems dependent on the species of origin. Mouse cells go on to form metastatic colonies whereas human colon cancer cells die. The difference is clearly due to the host response because prior treatment of the mice with cyclophosphamide obliterates the inhibitory response to human cells. This finding should be studied further.

GFP techniques have also shown that the CT-26 (mouse colon carcinoma) primary tumor inhibits the development of liver metastasis in BALB/c mice that receive intraportal injections of GFP-expressing tumor cells (11). Intravital microscopy of the livers of these mice showed that the growth of primary tumors promoted dormancy of single tumor cells for up to 7 days. Immunohistologic staining for Ki-67 confirmed that these solitary cells were indeed dormant. By contrast, in the absence of a primary tumor, GFP-expressing tumor cells quickly developed into micrometastases. Thus, primary CT-26 tumor implants seem to inhibit tumor metastasis by the promotion of a state of single-cell dormancy. Thus, both primary tumor and host may have defense mechanisms against tumor cells in the portal vein circulation.

Cyclophosphamide is a widely used cancer chemotherapy drug, including low-dose therapy (12). The results of the present study show that cyclophosphamide might, in certain instances, promote cancer cell growth as shown for the HCT-116 human colorectal cancer cells in the portal vein. Further studies into the sensitivity of host anticancer mechanisms to cyclophosphamide are indicated.

In conclusion, some cancer cells may be very sensitive to host mechanisms or the primary tumor when in the portal circulation, whereas other cancer cells seem resistant to this host mechanism. The host defense mechanism in the portal vein area is sensitive to cyclophosphamide. The implication of these results are important for understanding the tumor-host interaction of liver metastasis.

Acknowledgments

Received 8/18/2005; revised 10/3/2005; accepted 10/20/2005.

Grant support: NIH grant R21 CA109949-01 and American Cancer Society RSG-05-037-01-CCE (M. Bouvet) and National Cancer Institute grants CA099258, CA103563, and CA101600 (to AntiCancer, Inc.).

The costs of publication of this article were defrayed in part by the payment of page charges. This article must therefore be hereby marked *advertisement* in accordance with 18 U.S.C. Section 1734 solely to indicate this fact.

References

1. Hoffman RM. The multiple uses of fluorescent proteins to visualize cancer *in vivo*. Nat Rev Cancer 2005;5:796–806.
2. Chishima T, Miyagi Y, Wang X, et al. Cancer invasion and micrometastasis visualized in live tissue by green fluorescent protein expression. Cancer Res 1997;57:2042–7.
3. Yang M, Baranov E, Jiang P, et al. Whole-body optical imaging of green fluorescent protein-expressing tumors and metastases. Proc Natl Acad Sci U S A 2000;97:1206–11.
4. Yamauchi K, Yang M, Jiang P, et al. Real-time *in vivo* dual-color imaging of intracapillary cancer cell and nucleus deformation and migration. Cancer Res 2005;65:4246–52.
5. Lin WC, Pretlow TP, Pretlow TG 2nd, Culp LA. Bacterial lacZ gene as a highly sensitive marker to detect micrometastasis formation during tumor progression. Cancer Res 1990;50:2808–17.
6. Mook OR, Van Marle J, Vreeling-Sindelarova H, et al. Visualization of early events in tumor formation of eGFP-transfected rat colon cancer cells in liver. Hepatology 2003;38:295–304.
7. Wang J, Yang M, Hoffman RM. Visualizing portal vein metastatic trafficking to the liver with green fluorescent protein-expressing tumor cells. Anticancer Res 2004;24:3699–702.
8. Morris VL, MacDonald IC, Koop S, et al. Early interaction of cancer cells with the microvasculature in mouse liver and muscle during hematogenous metastasis: videomicroscope analysis. Clin Exp Metastasis 1993;11:377–90.
9. Yamamoto N, Jiang P, Yang M, et al. Cellular dynamics visualized in live cells *in vitro* and *in vivo* by differential dual-color nuclear-cytoplasmic fluorescent-protein expression. Cancer Res 2004;64:4251–6.
10. Kanda T, Sullivan KF, Wahl GM. Histone-GFP fusion protein enables sensitive analysis of chromosome dynamics in living mammalian cells. Curr Biol 1998;8:377–85.
11. Guba M, Cernaianu G, Koehl G, et al. A primary tumor promotes dormancy of solitary tumor cells before inhibiting angiogenesis. Cancer Res 2001;61:5575–9.
12. Man S, Bocci G, Francia G, et al. Antitumor effects in mice of low-dose (metronomic) cyclophosphamide administered continuously through the drinking water. Cancer Res 2002;62:2731–5.

Integrated physiology of proximal tubular organic anion transport

Naohiko Anzai, Promsuk Jutabha, Yoshikatsu Kanai and Hitoshi Endou

Purpose of review

Renal organic anion transport proteins play important roles in the reabsorption and the secretion of endogenous and exogenous compounds. This review focuses on the interpretation of the physiological integration of identified transport molecules in the renal proximal tubules.

Recent findings

To date, molecular identification of organic anion transport proteins is still continuing: rodent organic anion transporter 5, organic anion-transporting polypeptide 4C1, voltage-driven organic anion transporter 1, multidrug resistance-associated protein 4, and sodium-coupled monocarboxylate transporter have yielded additional information in this field. In addition, particularly at the apical membrane of the proximal tubules, the importance of the PDZ (PSD-95, DglA, and ZO-1) binding domain proteins has emerged in the formation of the multimolecular complex as a functional unit of membrane transport. Finally, discovery of dicarboxylate receptors in the renal tubular cells raises the possibility that dicarboxylate anions function as intrarenal signaling molecules. This novel aspect of renal organic anion transport, the potential modulation of signaling via dicarboxylate receptors, may be of significant relevance to renovascular hypertension and other renal diseases.

Summary

Comprehensive understanding of the multimolecular complex, which is composed of transporters and their related signaling elements and is supported by the scaffold proteins underneath the plasma membrane, may be useful in clarifying complex transport phenomena such as renal apical organic anion handling. In addition to the recent proteomics approaches and conventional molecular physiology, it is necessary to develop novel methods to analyze the overall function of the multimolecular complex for the post-genomic era.

Keywords

dicarboxylates, multimolecular complex, organic anion transporter, PDZ

Curr Opin Nephrol Hypertens 14:000–000. © 2005 Lippincott Williams & Wilkins.

Department of Pharmacology and Toxicology, Kyorin University School of Medicine, Tokyo, Japan

Correspondence to Hitoshi Endou, Department of Pharmacology and Toxicology, Kyorin University School of Medicine, 6-20-2 Shinkawa, Mitaka, Tokyo 181-8611, Japan
Tel: +81 422 47 5511 ext 3451; fax: +81 422 79 1321;
e-mail: endouh@kyorin-u.ac.jp

Current Opinion in Nephrology and Hypertension 2005, 14:000–000

Abbreviations

MRP	multidrug resistance-associated protein
NPT	sodium-phosphate transporter
NPT1	sodium-dependent phosphate cotransporter type 1
OAT	organic anion transporter
OAT-MMC	organic anion-transporting multimolecular complex
OATP	organic anion-transporting polypeptide
OATv1	voltage-driven organic anion transporter 1
PAH	*para*-aminohippurate
PDZ	PSD-95, DglA, and ZO-1
PEPT	peptide transporter
SMCT	sodium-coupled monocarboxylate transporter
SNP	single nucleotide polymorphism
URAT1	urate/anion exchanger

1062-4821

Introduction

In the kidney, proximal and distal tubules have two important roles: they remove waste products from the blood to the urine and at the same time they regulate the levels of many important substances in the blood. These functions of the renal tubules are achieved by a number of transporters and channels expressed at the apical and basolateral membranes of the tubular cells. Transporters and channels, expressed specifically in the appropriate domains of cell membranes, carry out bidirectional transport of their favored substrates across the tubular epithelial cells, and thus regulate the concentration and the equilibrium of these substrates.

Among the diverse transport systems in the kidney, the organic anion transport system has been the focus of particularly intensive scientific and medical interest, due to its roles in the excretion of many clinically important pharmaceuticals. During the last decade, molecular cloning approaches have identified several members of 'multispecific' organic anion transporter families which mediate the renal and hepatic elimination of organic anions, including the organic anion transporter (OAT), organic anion-transporting polypeptide (OATP), sodium-phosphate transporter (NPT), multidrug resistance-associated protein (MRP), and peptide transporter (PEPT) families. The transport mechanisms of renal organic anion transport have been reviewed in several recent articles [1°,2••,3,4••,5°,6–8]. In addition, several reviews have discussed the urate transport mechanism in the kidney [9°,10••,11]. This review will focus on the current knowledge of molecular aspects of renal OATs, particularly apical transporters, and will introduce the novel idea that the multimolecular complex is composed of transporters and their regulating proteins and is

assembled by scaffold proteins which are responsible for the transmembrane transport of organic anions.

Novel aspects of renal organic anion transporters

To date, molecular identification and functional characterization of organic anion transport proteins in the kidney is still continuing.

Organic anion transporter family

The basolateral organic anion transport system in the kidney has been extensively investigated by in-vitro experiments such as membrane vesicles and by in-vivo experiments. Molecular identification and functional characterization of two organic anion/dicarboxylate exchangers, OAT1 and OAT3, whose characteristics correspond well to those observed in classical studies of organic anion transport, has led to a better understanding of the basolateral organic anion transport system, although the exit path for organic anions has still not been clarified [2••,6]. In contrast, little is known about the apical organic anion transport system. In particular, the physiological role of OAT4 [12], the first apical isoform of the OAT family to be identified, is unclear, although several apical organic anion transporters have been cloned (Fig. 1). We recently reported that OAT4 is not a facilitated transporter but an organic anion/dicarboxylate exchanger that mediates bidirectional organic anion transport [13••]. These results indicate that OAT4 is a renal apical organic anion/dicarboxylate exchanger, serving mainly as a tubular reabsorptive pathway for organic anions including sulfate conjugates, driven by an outwardly directed gradient of dicarboxylates such as α-ketoglutarate. It seems unlikely that two exchangers of the same type existing in both sides of a membrane lead to the vectorial transport of organic anions, as Schmitt and Burckhardt [14] discussed in the case of bovine brush-border membrane vesicles. To separate or isolate the organic anion transport at the apical membrane of proximal tubules from that at the basolateral membrane, both transporters may have different transport characteristics.

Figure 1. Transepithelial transport of organic anions (OAs) in renal proximal tubules

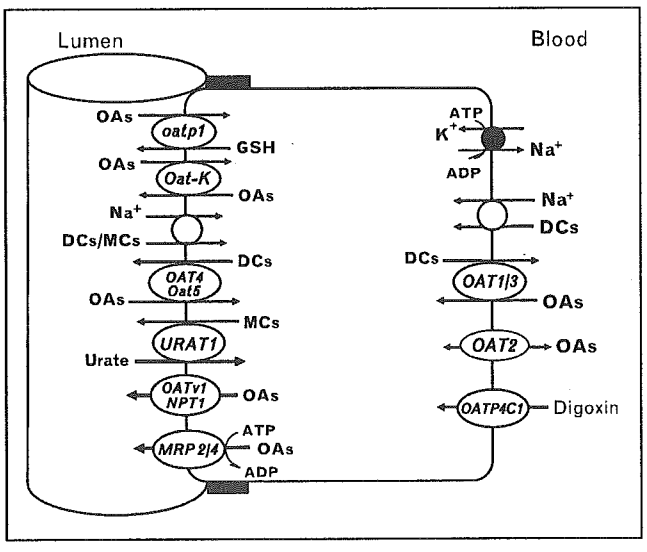

Organic anion transporter (OAT) isoforms OAT1 and OAT3, the main entrance pathways for organic anions in exchange for dicarboxylates (DCs), as well as OAT2 and OATP4C1, are expressed in the basolateral membrane. In contrast, several kinds of organic transport proteins are identified in the apical membrane, such as oatp1, Oat-K, Na^+-anion cotransporter (NaDC1, SMCT), OAT4 and rodent Oat5, urate/anion exchanger (URAT1), sodium-dependent phosphate cotransporter type 1 (NPT1)/pig voltage-driven organic anion transporter 1 (OATv1), and multidrug resistance-associated protein 2/4 (MRP2/4). MC, monocarboxylate such as lactate or nicotinate.

Functional characterization of rodent Oat5 introduced a novel idea concerning this issue. Mouse Oat5 [15] and rat Oat5 (rOat5) [16] are functional but not the same as nonfunctional human OAT5 reported by Sun *et al.* [17]. We also found that rOat5 is localized at the apical membrane of the late segment of proximal tubules and mediates the sodium-independent transport of sulfate conjugates of steroids such as estrone-3-sulfate (E_1S) and dehydroepiandrosterone sulfate, as well as ochratoxin A. The most surprising finding of our study is that rOat5 interacted not only with the five-carbon dicarboxylate α-ketoglutarate (C5), but also with the four-carbon dicarboxylate succinate (C4), which has not been reported as a counterion for the classical renal organic anion transport system to date; rOat5 thus mediates organic anion/succinate exchange (N. Anzai, P. Jutabha, A. Enomoto *et al.*, unpublished observation). The interaction with C4 succinate is not found in the basolateral OAT isoform OAT3. These data indicate that rOat5 is the first renal organic anion transporter that may function mainly as an apical pathway for the reabsorption of some organic anions driven by an outward gradient of both α-ketoglutarate and succinate. It seems appropriate that the apical isoforms of OAT utilize C4 succinate as a counterion, whereas the basolateral OATs utilize C5 α-ketoglutarate as a counterion (Fig. 2) to separate the transport of organic anions at both sides of proximal tubular cells. This idea is supported by the results that the apical membrane isoform OAT4-mediated transport was inhibited by succinate as well as glutarate (P. Jutabha, N. Anzai, H. Endou *et al.*, unpublished observation). Interestingly, urate transport via the urate/anion exchanger (URAT1) localized at the renal apical membrane was also inhibited by succinate at a millimolar concentration in the *Xenopus* oocyte system [18]. It has been suggested that succinate exchange in addition to α-ketoglutarate exchange is a common mechanism for the apical membrane isoforms of OAT family members.

Figure 2. Proposed scheme of organic anion (OA) transport coupling with two dicarboxylates in the proximal tubules

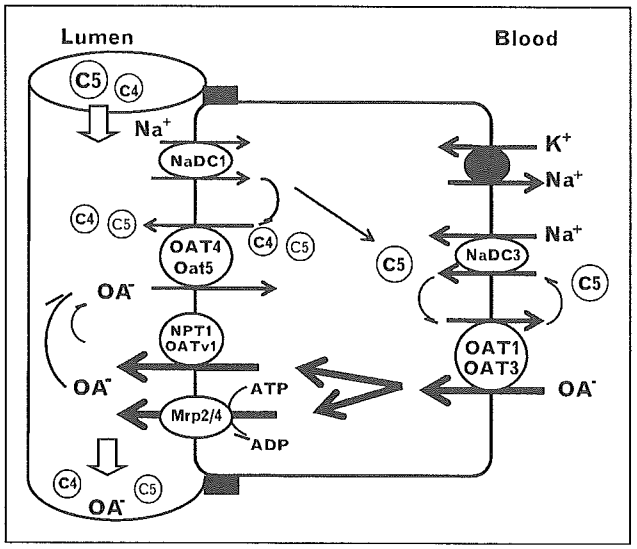

Basolateral organic anion transporter (OAT) isoforms OAT1 and OAT3 accept only five-carbon dicarboxylate (DC) α-ketoglutarate (C5), while apical OAT isoforms human OAT4 and rodent Oat5 accept four-carbon dicarboxylate succinate (C4) in addition to C5 α-ketoglutarate. Glomerular filtrated dicarboxylates are reabsorbed by Na^+-anion cotransporter NaDC1 and some of them are backfluxed to the tubular lumen, due to the function of apical OA/DC exchanger OAT4 or Oat5, which may contribute to retrieving the secreted organic anions such as steroid sulfates by efflux transporter multidrug resistance-associated protein 2/4 (MRP2/4) and sodium-dependent phosphate cotransporter type 1 (NPT1). OATv1, voltage-driven organic anion transporter 1.

Organic anion-transporting polypeptide family

OATPs/oatps are a group of membrane solute carriers with a wide spectrum of amphipathic transport substrates. Recent reviews deal with this subject extensively [19•,20,21]. Several members of the OATP family, such as oatp1 and Oat-K1/K2, are located in the apical membrane of proximal tubules (Fig. 1), where they have been suggested to play a role in the secretion/reabsorption of selected anionic substrates [2••,22]. Recently, Mikkaichi *et al.* [23•] have isolated an OAT (OATP4C1) from human kidney. Human OATP4C1 is the first member of the OATP family expressed in human kidney [23•]. Its rat counterpart, Oatp4c1, also isolated from rat kidney, is localized at the basolateral membrane of the proximal tubule cells. Human OATP4C1 transports cardiac glycosides (digoxin, Michaelis-Menten constant (Km) 7.8 μM and ouabain, Km 0.38 μM), thyroid hormone (triiodothyronine, Km 5.9 μM and thyroxine), cAMP, and methotrexate in a sodium-independent manner. Rat Oatp4c1 also transports digoxin (Km 8.0 μM) and triiodothyronine (Km 1.9 μM). These data suggest that human OATP4C1/rat Oatp4c1 may be the first step of the transport pathway of digoxin and various compounds into urine in the kidney.

Sodium-phosphate transporter family

Molecular studies have determined that type I phosphate transporters (SLC17), a family of proteins initially characterized as phosphate carriers, are expressed at the apical membrane of renal proximal tubular cells and mediate the transport of organic anions (Fig. 1) [2••,24•]. Mouse and human sodium-dependent phosphate cotransporter type 1 (NPT1) was shown to mediate the transport of various organic anions in a chloride-dependent manner. Moreover, because human NPT1 exhibits an affinity for *para*-aminohippurate (PAH), corresponding to previous reports using brush-border membrane vesicles, NPT1 is also suggested to represent the classical voltage-dependent PAH transporter [8]. An influence of the membrane potential on PAH transport, however, was not demonstrated [25]. We isolated a novel transport protein with the properties of voltage-driven organic anion transport from pig kidney cortex by expression cloning in *Xenopus* oocytes [26]. A cDNA encoding a 467-amino-acid peptide was designated as OATv1 (voltage-driven organic anion transporter 1). The predicted amino acid sequence of OATv1 exhibited 60–65% identity to those of human, rat, rabbit, and mouse NPT1. OATv1 mediates the transport of PAH, E_1S, estradiol-17-β-glucuronide, and urate. PAH transport via PATv1 was affected by the changes in membrane potential. This transport protein is localized at the apical membrane of the renal proximal tubule, consistent with the proposed localization of a voltage-driven organic anion transporter. Therefore, it is suggested that OATv1 plays an important role in excreting various organic anions, including PAH and urate, driven by membrane voltage through the apical membrane of the tubular epithelial cells into the urine.

Multidrug resistance-associated protein family

The MRP family is composed of nine related ABC transporters that are able to transport structurally diverse lipophilic anions and function as drug efflux pumps [27]. Among them, MRP2 and MRP4 were well investigated because they are the only members expressed at the apical membrane of kidney proximal tubules (Fig. 1). Recently, MRP4 has been proposed to mediate secretion of various organic anions such as cAMP, cGMP, and PAH across the apical membrane of human renal proximal tubular cells [28,29••]. van Aubel *et al.* [30••] demonstrated that MRP4, but not apical MRP2, mediates ATP-dependent urate transport via a positive cooperative mechanism (Km = 1.5 mM, Vmax = 47 pmol/mg/min, and Hill coefficient = 1.7). They proposed MRP4 as a candidate transporter for urinary urate excretion and suggested that MRP4 may also mediate hepatic export of urate into the circulation, because of its basolateral expression in the liver (Fig. 1).

Apical sodium-anion influx transporter

As we reported previously, URAT1 transports urate in exchange for intracellular organic anions such as lactate, nicotinate, and the antiuricosuric drug metabolite pyrazinecarboxylate [18]. Intracellular organic anions are made available by their uptake from the glomerular filtrate across the luminal membrane, uptake from peritubular capillaries by basolateral transporters (OATs), and cell metabolism [31]. Thus, the substances that provide counter ions for URAT1 at the apical membrane of proximal tubular cells had not been identified. Recently, Ganapathy and his colleagues sequentially reported that SLC5A8, a candidate tumor suppressor gene that is silenced in colon cancer in humans, is a sodium-coupled monocarboxylate transporter (SMCT). SMCTs transport lactate, nicotinate (both substances are counterions for URAT1) and short-chain fatty acids [32,33••,34•,35•]. Through the Na^+-coupled reabsorption of lactate, the counterion for URAT1, the modulation of SMCT function may affect URAT1-mediated urate transport. This was preliminarily reported by Zandi-Nejad *et al.* [36]. They showed marked stimulation of urate uptake by pre-exposure of pyrazinecarboxylate and nicotinate in the *Xenopus* oocytes coinjected with Slc5a8 and URAT1. SLC5A8 (SMCT) seems another good target in drug development for the treatment of hyperuricemia and gout.

Molecular integration of renal apical organic anion transporters

The importance of PDZ (PSD-95, DglA, and ZO-1) proteins of the proximal tubules has emerged for multimolecular complex formation as a functional unit of membrane transport.

PDZ proteins and proximal tubular organic anion transport

PDZ-binding domains have been identified in various proteins and are known to be modular protein–protein recognition domains that play a role in protein targeting and protein complex assembly [37]. These domains range from 80 to 90 amino acids in length and typically bind to proteins containing the tripeptide motif (S/T)–X–Ø (X = any amino acid and Ø = a hydrophobic residue) at their C-termini. These multidomain molecules not only target and provide scaffolds for protein–protein interactions but also modulate the function of receptors and ion channels, by which they associate. In recent years, several PDZ proteins such as NHERF1, NHERF2, and PDZK1 have been identified in the proximal tubules and they are thought to be important for the generation and maintenance of epithelial polarity and the formation of large protein complexes [38••,39••,40].

A newly found genetic alteration in *SLC22A12* from an idiopathic renal hypouricaemia patient has prompted us to consider the importance of the URAT1 extreme intracellular C-terminal region for its function. A 5 bp deletion near the URAT1 C-terminal end (1639–1643 del) causes frameshift and the seven amino acids in the terminal sequences have changed into eight different amino acids [41]. The URAT1 transport activity of this mutation is low in the *Xenopus* oocyte expression system. Interestingly, the PDZ binding motif at the C-terminal end of URAT1 disappears following this amino acid sequence modification. Thus, we initiated a yeast two-hybrid approach to investigate the putative URAT1-associated proteins that modulate its transport function, identifying the multivalent PDZ domain-containing protein PDZK1 as an apparent partner of URAT1 in the human kidney [42••]. Moreover, URAT1 transport activities were increased by coexpression of PDZK1 in transfected HEK293 cells. We speculated that PDZK1 stabilizes or anchors URAT1 at the cell membrane, making it less likely to be internalized and subsequently degraded. During the course of the URAT1–PDZK1 interaction study, we also identified the interaction between OAT4 and two PDZ proteins, PDZK1 and NHERF1 [42••,43]: that of PEPT2 to PDZK1 [44], and that of NPT1 to both PDZK1 and NHERF1 (P. Jutabha, N. Anzai, Y. Kanai *et al.*, unpublished observation), with functional consequences. It has been proposed that the organic anion transporters, such as MRP2/4, NPT1, PEPT2, Oatp1, and Oat-k1/k2, which localize to the apical membrane and have the consensus PDZ-motif sequence at their C-termini, target the apical membrane mediated by PDZ domain-containing proteins [8]. In addition to our results, Gisler *et al.* performed the yeast two-hybrid screens using single PDZ domains derived from mouse PDZK1 (NaPi-Cap1) as bait. They reported that, besides NaPi-IIa, mouse PDZK1 interacts with many other membrane transporters including renal-specific transporter (mouse URAT1 [45]) in the brush border of proximal tubular cells [46] and with intracellular signaling elements [47]. Furthermore, Kato *et al.* [48] tested directly the interaction between several xenobiotic transporters, including PEPT1/2, OATPs and OAT4 as bait and four PDZ proteins (NHERF1/2, PDZK1, IKEPP) as prey. Although most of these interactions lack information on their functional consequences, the combination of these studies and the results discussed above indicate the physiological significance of the interaction between apical OATs and PDZ proteins in the proximal tubule.

Multimolecular assembly of transport proteins at the plasma membrane

In the last few years, many studies on the PDZ interaction network have been performed in kidney proximal tubules [38••,39••]. In kidneys, the proximal tubule has important roles for both the reabsorption of filtered substances and the secretion of water-soluble drugs, toxins,

and metabolic waste products. These two opposite transport directions are simultaneously accomplished by the coordinated action of ion channels and transporters located both in the apical and basolateral membrane. Thus, the polarized expression of these membrane proteins is essential for the function of the proximal tubular cells. Scaffolding proteins underneath the plasma membrane, such as PDZ proteins, are thought to contribute to generating cell polarity by the formation of a junctional complex and by protein anchoring. In addition, proximal tubular transport processes are regulated by a number of factors, including hormones such as parathyroid hormone. For efficient and specific signal transduction, for the enhancement of membrane expression, and for the direct modulation of transport processes, the formation of functional complexes, including transport proteins, hormonal receptors, and intracellular signaling elements, is beneficial. This supramolecular structure, supported by scaffolds such as PDZ proteins, is proposed to be an ultimate functional unit of membrane transport (Fig. 3).

Organic anion-transporting multimolecular complex at the renal apical membrane

Although the introduction of molecular approaches has led to the identification of several transport molecules and to the examination of single transport protein activity, the precise mechanisms of renal apical handling of various organic anions are largely unknown. Application of the novel proteomics approaches based on the concept of an organic anion-transporting multimolecular complex (OAT-MMC) may, however, contribute to the comprehensive understanding of the apical organic anion transport phenomenon in the proximal tubules. Moe [49] suggested in his short commentary that this scaffold provides a platform for regulated apical urate uptake based on the ability of PDZK1 to cluster two urate-transporting proteins NaPi-I (mouse NPT1) and URAT1. This coupling may be one of the components of the apical urate-transporting molecular complex (URAT-MMC). We have already observed that the SMCT C-terminal that has the PDZ motif (–T–R–L) binds to NHERF1 but not to PDZK1 (N. Anzai, unpublished observation) and Gisler *et al.* [46] reported the interaction between PDZK1 and NHERF1. Coupling between URAT1 and SMCT through two PDZ proteins can thus form a single complex. The urate efflux transporter MRP4 also contains a PDZ motif at its C-terminal (–T–A–L), and is likely to interact in a similar fashion with PDZ proteins. With other unknown signaling elements, apical URAT-MMC is composed of several membrane transporters with opposite transport directions and PDZ scaffolds (Fig. 4A). It may also be responsible for the concerted regulation of urate transport at the apical membrane. With respect to other organic anions, NPT1, MRP2/4, OAT4, and NaDC1 (which needs NHERF2 for the SGK effect, although its C-terminal is thought to be on the extracellular side [50]) are the main components of an apical OAT-MMC with other unknown factors (Fig. 4B). In both molecular complexes, OAT family members such as URAT1 and OAT4 seem to be important constituents for the determination of the net flux of the substrates, as dictated by the bidirectional nature of their transport.

Figure 3. Schematic diagram of the functional unit of membrane transport

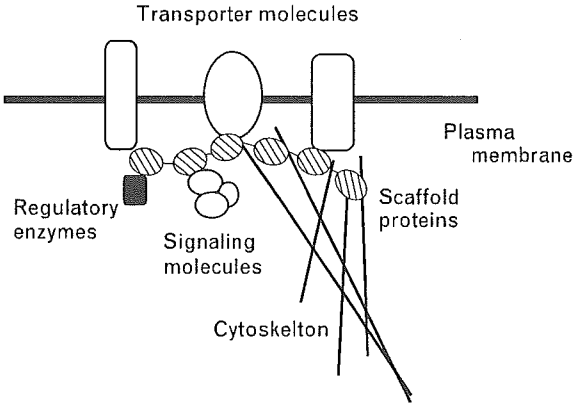

Clustering of several transport molecules, including regulatory enzymes, signaling molecules and cytoskeleton, is thought to be mediated by multidomain scaffold protein.

Is apical organic anion-transporting multimolecular complex the regulator of dicarboxylate signaling?

Recently, the receptors for dicarboxylates, such as succinate and α-ketoglutarate, have been identified in the kidneys [51••]. Succinate is a natural ligand for GPR91, and α-ketoglutarate is that of GPR99, orphan G-protein-coupled receptors (GPCRs) in the proximal and distal tubules. He *et al.* [51••] showed that succinate increases blood pressure in mice and that the succinate-induced hypertension involves the renin–angiotensin system. These findings raise the possibility that the dicarboxylate concentration surrounding proximal tubular cells, determined by the balance between the uptake of dicarboxylates via Na^+-dependent dicarboxylate transporters (NaDCs) and their efflux via OATs, is an important factor that regulates renovascular hypertension. In the earlier part of this review, we proposed that OAT4 seems to contribute to the tubular reabsorption of organic anions, taking the existence of the outwardly directed dicarboxylate gradient in the tubular cells into account. Not only the organic anion influx, however, but also the dicarboxylate efflux seem to have important roles for OAT family members, because, to date, there is no other transport protein mediating the dicarboxylate efflux. Due to the function of apical OAT-MMC, dicarboxylates remaining in the tubular fluid go down to the distal nephron and function as a signaling molecule for renovascular hypertension, a disease closely linked to

Figure 4. Schematic presentation of transporting multimolecular complexes at the apical membrane of the proximal tubule

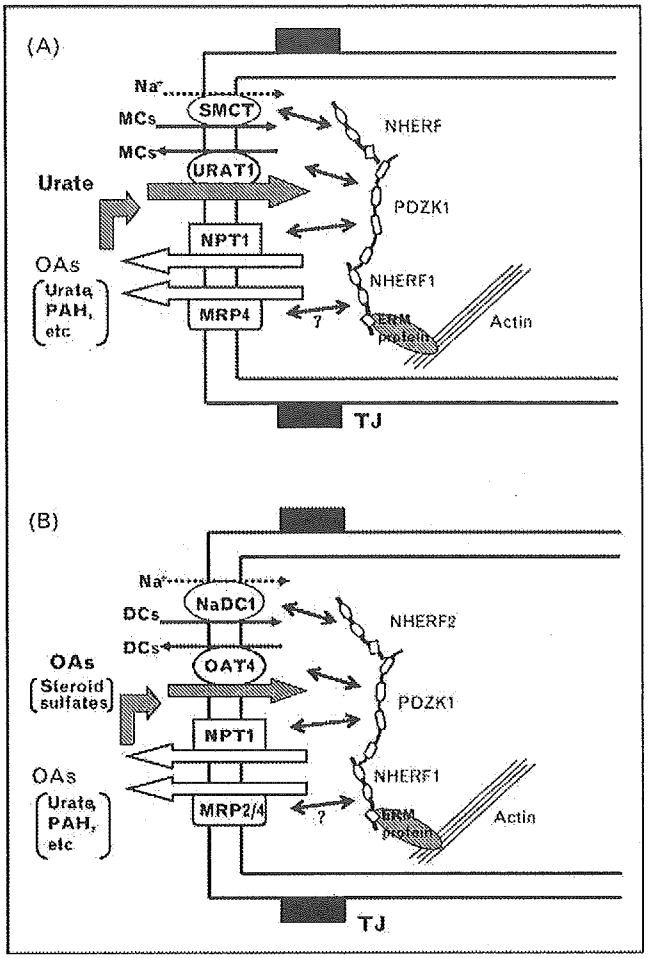

(A) Apical urate-transporting multimolecular complex (URAT-MMC) is composed of urate/anion exchanger (URAT1), sodium-coupled monocarboxylate transporter (SMCT), sodium-dependent phosphate cotransporter type 1 (NPT1), and multidrug resistance-associated protein 4 (MRP4) scaffolded by the PDZ (PSD-95, DgIA, and ZO-1) protein network (NHERF1/2, PDZK1) underneath the plasma membrane. (B) Apical organic anion-transporting multimolecular complex (OAT-MMC) is composed of OAT4, NaDC1, NPT1, and MRP2/4 scaffolded by the PDZ protein network (NHERF1/2, PDZK1). MC, monocarboxylate such as lactate or nicotinate; PAH, *para*-aminohippurate; TJ, tight junction.

atherosclerosis, diabetes and renal failure. Apical OAT-MMC, therefore, can function as a regulator of dicarboxylate signaling and could be a novel therapeutic target for such disease processes. From this point of view, a potential role for OATs in renal ischemic injury, proposed by Eraly *et al.* [7], has become practical these days and should be evaluated extensively based on our concept of the transporting molecular complex.

Conclusion

Understanding the overall function of a transporting molecular complex is essential when explaining cellular functions based on the functions of each transporter molecule. The application of this concept may be useful in understanding the complex phenomena that underlie the vectorial transport of organic anions in the renal proximal tubules. Several steps are needed, however, to clarify all the components and their networks. New technologies or theoretical modelings may be necessary to analyze the whole system. The first step is the dissection of the molecular complex components using proteomics approaches. Precise characterizations of component molecules and their interactions are of course indispensable. Nowadays, the importance of drug transporter single nucleotide polymorphisms (SNPs) is emphasized as a determinant of inter-individual differences in drug response [52•,53]. SNPs with altered function have recently been reported in PEPT2 [54•] and OAT1 [55•]. We tested the interaction of URAT1 C-terminus with two PDZK1 SNPs (Y145H and V372E) and found that Y145H, which involves a mutation in the PDZ domain, lacks the binding affinity in surface plasmon resonance assay [56]. This suggests that genetic polymorphisms should also be evaluated under the idea of a transporting molecular complex. Finally, the identification of dicarboxylate GPCR in the distal tubules prompted us to investigate the organic anion transporter(s) in that segment, although there are few studies that have examined distal tubular organic anion transport. We have found, however, that a new isoform of an OAT member is localized in the collecting duct cells [57]. Similar to inorganic ion transporters such as sodium, the transport of organic anions in the distal nephron may contribute to the fine-tuning of urinary secretion. It thus seems equally important to clarify the function of the OAT-MMC in the distal nephron.

Acknowledgements

The authors wish to thank all the members of their laboratories who have contributed much of the work discussed in this review. This work was supported in part by grants from the Japanese Ministry of Education, Culture, Sports, Science and Technology, the Science Research Promotion Fund of the Japan Private School Promotion Foundation, Grants-in-Aids for Scientific Research from the Japan Society for the Promotion of Science (JSPS), Grants-in-Aid from the Nakatomi Foundation, the Salt Science Research Foudation No. 0524, the Japan Foundation of Applied Enzymology, and Health and Labor Sciences Research Grants for Research on Advanced Medical Technology: Toxicogenomics Project. PJ is a research fellow supported by the Labor Sciences Research Grants for Research on Advanced Medical Technology: Toxicogenomics Project.

References and recommended reading

Papers of particular interest, published within the annual period of review, have been highlighted as:
- • of special interest
- •• of outstanding interest

1 • Miyazaki H, Sekine T, Endou H. The multispecific organic anion transporter family: properties and pharmacological significance. Trends Pharmacol Sci 2004; 25:654–662.
This paper tracks the current progress of the OAT family from a pharmacological point of view.

2 •• Wright SH, Dantzler WH. Molecular and cellular physiology of renal organic cation and anion transport. Physiol Rev 2004; 84:987–1049.
This is an excellent review of the extensive physiological literature on the renal organic anion and cation transport systems.

3 You G. The role of organic ion transporters in drug disposition: an update. Curr Drug Metab 2004; 5:55–62.

4 •• Eraly SA, Bush KT, Sampogna RV, *et al.* The molecular pharmacology of organic anion transporters: from DNA to FDA? Mol Pharmacol 2004; 65:479–487.
This is an intriguing review on several molecular aspects of the OAT family.

5 • Koepsell H, Endou H. The SLC22 drug transporter family. Pflügers Arch 2004; 447:666–676.
This is a standard general review of the organic cation/anion/zwitterions transporter family.

6 Bruckhardt BC, Bruckhardt G. Transport of organic anions across the basolateral membrane of proximal tubule cells. Rev Physiol Biochem Pharmacol 2003; 146:95–158.

7 Eraly SA, Blantz RC, Bhatnagar V, Nigam SK. Novel aspects of renal organic anion transporters. Curr Opin Nephrol Hypertens 2003; 12:551–558.

8 Russel FG, Masereeuw R, van Aubel RA. Molecular aspects of renal anionic drug transport. Annu Rev Physiol 2002; 64:563–594.

9 • Anzai N, Enomoto A, Endou H. Renal urate handling: clinical relevance of recent advances. Curr Rheumatol Rep 2005; 7:227–234.
This is a concise review focusing on the urate transport system in the kidneys.

10 •• Hediger MA, Johnson RJ, Miyazaki H, Endou H. Molecular physiology of urate transport. Physiology (Bethesda) 2005; 20:125–133.
This is an extensive review on the urate transport including the physiological importance of urate in the body.

11 Rafey MA, Lipkowitz MS, Leal-Pinto E, Abramson RG. Uric acid transport. Curr Opin Nephrol Hypertens 2003; 12:511–516.

12 Cha SH, Sekine T, Kusuhara H, *et al.* Molecular cloning and characterization of multispecifc organic anion transporter 4 expressed in the placenta. J Biol Chem 2000; 275:4507–4512.

13 •• Ekaratanawong S, Anzai N, Jutabha P, *et al.* Human organic anion transporter 4 is a renal apical organic anion/dicarboxylate exchanger in the proximal tubules. J Pharmacol Sci 2004; 94:297–304.
This paper provides the first description that apical OAT isoform functions as an organic anion/dicarboxylate exchanger.

14 Schmitt C, Burckhardt G. p-Aminohippurate/2-oxoglutarate exchange in bovine renal brush-border and basolateral membrane vesicles. Pfluegers Arch 1993; 423:280–290.

15 Youngblood GL, Sweet DH. Identification and functional assessment of the novel murine organic anion transporter Oat5 (Slc22a19) expressed in kidney. Am J Physiol Renal Physiol 2004; 287:F236–F244.

16 Hirata T, Jutabha P, Anzai N, *et al.* Characterization of a novel rat organic anion transporter OAT5 as an organic anion/dicarboxylate exchanger at the apical membrane of renal proximal tubules [abstract]. FASEB J 2004; 18:1250.

17 Sun W, Wu RR, van Poelje PD, Erion MD. Isolation of a family of organic anion transporters from human liver and kidney. Biochem Biophys Res Commun 2001; 283:417–422.

18 Enomoto A, Kimura H, Chairoungdua A, *et al.* Molecular identification of a renal urate anion exchanger that regulates blood urate levels. Nature 2002; 417:447–452.

19 • Hagenbuch B, Meier PJ. Organic anion transporting polypeptides of the OATP/ SLC21 family: phylogenetic classification as OATP/ SLCO superfamily, new nomenclature and molecular/functional properties. Pflugers Arch 2004; 447:653–665.
This is a standard general review of the organic anion transporting family.

20 Mikkaichi T, Suzuki T, Tanemoto M, *et al.* The organic anion transporter (OATP) family. Drug Metab Pharmacokinet 2004; 19:171–179.

21 van Montfoort JE, Hagenbuch B, Groothuis GM, *et al.* Drug uptake systems in liver and kidney. Curr Drug Metab 2003; 4:185–211.

22 Masuda S. Functional characteristics and pharmacokinetic significance of kidney-specific organic anion transporters, OAT-K1 and OAT-K2, in the urinary excretion of anionic drugs. Drug Metab Pharmacokinet 2003; 18:91–103.

23 • Mikkaichi T, Suzuki T, Onogawa T, *et al.* Isolation and characterization of a digoxin transporter and its rat homologue expressed in the kidney. Proc Natl Acad Sci U S A 2004; 101:3569–3574.
This paper provides evidence that human OATP4C1 is a renal digoxin transporter.

24 • Reimer RJ, Edwards RH. Organic anion transport is the primary function of the SLC17/type I phosphate transporter family. Pflugers Arch 2004; 447:629–635.
This is a standard general review of the vesicular glutamate transporter family.

25 Uchino H, Tamai I, Yamashita K, *et al.* p-Aminohippuric acid transport at renal apical membrane mediated by human inorganic phosphate transporter NPT1. Biochem Biophys Res Commun 2000; 270:254–259.

26 Jutabha P, Kanai Y, Hosoyamada M, *et al.* Identification of a novel voltage-driven organic anion transporter present at apical membrane of renal proximal tubule. J Biol Chem 2003; 278:27930–27938.

27 Kruh GD, Belinsky MG. The MRP family of drug efflux pumps. Oncogene 2003; 22:7537–7552.

28 van Aubel RA, Smeets PH, Peters JG, *et al.* The MRP4/ABCC4 gene encodes a novel apical organic anion transporter in human kidney proximal tubules: putative efflux pump for urinary cAMP and cGMP. J Am Soc Nephrol 2002; 13:595–603.

29 •• Smeets PH, van Aubel RA, Wouterse AC, *et al.* Contribution of multidrug resistance protein 2 (MRP2/ABCC2) to the renal excretion of p-aminohippurate (PAH) and identification of MRP4 (ABCC4) as a novel PAH transporter. J Am Soc Nephrol 2004; 15:2828–2835.
This paper provides evidence that human MRP4 is a renal PAH transporter.

30 •• van Aubel RA, Smeets PH, van den Heuvel JJ, Russel FG. Human organic anion transporter MRP4 (ABCC4) is an efflux pump for the purine end metabolite urate with multiple allosteric substrate binding sites. Am J Physiol Renal Physiol 2005; 288:F327–F333.
This paper provides evidence that human MRP4 is a renal urate transporter.

31 Roch-Ramel F, Werner D, Guisan B. Urate transport in brush-border membrane of human kidney. Am J Physiol Renal Physiol 1994; 266:F797–F805.

32 Miyauchi S, Gopal E, Fei YJ, Ganapathy V. Functional identification of SLC5A8, a tumor suppressor down-regulated in colon cancer, as a Na(+)-coupled transporter for short-chain fatty acids. J Biol Chem 2004; 279:13293–13296.

33 •• Gopal E, Fei YJ, Sugawara M, *et al.* Expression of slc5a8 in kidney and its role in Na(+)-coupled transport of lactate. J Biol Chem 2004; 279:44522–44532.
This paper describes the functional characteristics of the sodium–glucose cotransporter family member SLC5A8.

34 • Gopal E, Fei YJ, Miyauchi S, *et al.* Sodium-coupled and electrogenic transport of B-complex vitamin nicotinic acid by slc5a8, a member of the Na/glucose co-transporter gene family. Biochem J 2005; 388:309–316.
This paper describes the functional characteristics of the sodium–glucose cotransporter family member SLC5A8.

35 • Ganapathy V, Gopal E, Miyauchi S, Prasad PD. Biological functions of SLC5A8, a candidate tumour suppressor. Biochem Soc Trans 2005; 33:237–240.
This paper describes the functional characteristics of the sodium-glucose cotransporter family member SLC5A8.

36 Zandi-Nejad K, Plata C, Enck AH, *et al.* Slc5a8 functions as a sodium-dependent pyrazionate and nicotinate cotransporter: implications for renal urate transport [abstract]. J Am Soc Nephrol 2004; 15:89A.

37 Hung AY, Sheng M. PDZ domains: structural modules for protein complex assembly. J Biol Chem 2002; 277:5699–5702.

38 •• Brone B, Eggermont J. PDZ proteins retain and regulate membrane transporters in polarized epithelial cell membranes. Am J Physiol Cell Physiol 2005; 288:C20–C29.
This is an excellent and comprehensive review of the importance of PDZ interaction in the epithelial cells.

39 •• Hernando N, Wagner CA, Gisler SM, *et al.* PDZ proteins and proximal ion transport. Curr Opin Nephrol Hypertens 2004; 13:569–574.
This is an excellent and concise review of the importance of PDZ interaction in the proximal tubular cells.

40 Biber J, Gisler SM, Hernando N, *et al.* PDZ interactions and proximal tubular phosphate reabsorption. Am J Physiol Renal Physiol 2004; 287:F871–F875.

41 Ichida K, Hosoyamada M, Hisatome I, *et al.* Clinical and molecular analysis of patients with renal hypouricemia in Japan: influence of URAT1 gene on urinary urate excretion. J Am Soc Nephrol 2004; 15:164–173.

42 •• Anzai N, Miyazaki H, Noshiro R, *et al.* The multivalent PDZ domain-containing protein PDZK1 regulates transport activity of renal urate-anion exchanger URAT1 via its C-terminal. J Biol Chem 2004; 279:45942–45950.
This study describes, for the first time, the interaction of OAT family members (URAT1 and OAT4) with the PDZ domain protein PDZK1 and its functional consequences.

43 Miyazaki H, Anzai N, Jutabha P, *et al.* Transport mechanisms of a renal apical drug transporter, organic anion transporter 4 [abstract]. J Pharmacol Sci 2004; 94:112P.

44 Anzai N, Noshiro R, Miyazaki H, *et al.* Identification of the intracellular binding protein with proton-coupled oligopeptide transporter PEPT2 using yeast two-hybrid assay [abstract]. FASEB J 2004; 18:A695.

45 Hosoyamada M, Ichida K, Enomoto A, *et al.* Function and localization of urate transporter 1 in mouse kidney. J Am Soc Nephrol 2004; 15:261–268.

46 Gisler SM, Pribanic S, Bacic D, *et al.* PDZK1. I: A major scaffolder in brush borders of proximal tubular cells. Kidney Int 2003; 64:1733–1745.

47 Gisler SM, Madjdpour C, Bacic D, *et al.* PDZK1. II: An anchoring site for the PKA-binding protein D-AKAP2 in renal proximal tubular cells. Kidney Int 2003; 64:1746–1754.

48 Kato Y, Yoshida K, Watanabe C, *et al.* Screening of the interaction between xenobiotic transporters and PDZ proteins. Pharm Res 2004; 21:1886–1894.

49 Moe OW. Scaffolds: orchestrating proteins to achieve concerted function. Kidney Int 2003; 64:1916–1917.

50 Boehmer C, Embark HM, Bauer A, *et al.* Stimulation of renal Na^+-dicarboxylate cotransporter 1 by Na^+/H^+ exchanger regulating factor 2, serum and glucocorticoid inducible kinase isoforms, and protein kinase B. Biochem Biophys Res Commun 2004; 313:998–1003.

51 •• He W, Miao FJ, Lin DC, *et al.* Citric acid cycle intermediates as ligands for orphan G-protein-coupled receptors. Nature 2004; 429:188–193.
This paper provides evidence that GPR91 and GPR99 are expressed in the kidneys and function as dicarboxylate receptors.

52 • Ishikawa T, Tsuji A, Inui K, *et al.* The genetic polymorphism of drug transporters: functional analysis approaches. Pharmacogenomics 2004; 5:67–99.
This review emphasizes drug transporter SNPs as a determinant of inter-individual differences in drug response.

53 Marzolini C, Tirona RG, Kim RB. Pharmacogenomics of the OATP and OAT families. Pharmacogenomics 2004; 5:273–282.

54 • Terada T, Irie M, Okuda M, Inui K. Genetic variant Arg57His in human H^+/peptide cotransporter 2 causes a complete loss of transport function. Biochem Biophys Res Commun 2004; 316:416–420.
This paper provides the first description about the altered function of PEPT2 SNPs.

55 • Fujita T, Brown C, Carlson EJ, *et al.* Functional analysis of polymorphisms in the organic anion transporter, SLC22A6 (OAT1). Pharmacogenet Genomics 2005; 15:201–209.
This paper provides the first description of the altered function of OAT1 SNPs.

56 Anzai N, Miyazaki H, Hirata T, *et al.* Regulation of renal urate transporter URAT1 transport function by PDZ domain protein PDZK1 [abstract]. J Pharmacol Sci 2005; 97:120P.

57 Yokoyama H, Anzai N, Chaekuntode S, *et al.* Identification of a novel organic anion transporter OAT8 from the rat kidney [abstract]. Nephrol Dial Transpl 2003; 18:S8.

Available online at www.sciencedirect.com
SCIENCE DIRECT®
Biochimica et Biophysica Acta 1720 (2005) 44 – 51
BIOCHIMICA ET BIOPHYSICA ACTA
BBA
http://www.elsevier.com/locate/bba

Functional expression of the rat organic anion transporter 1 (rOAT1) in *Saccharomyces cerevisiae*

Suphansa Sawamiphak [a], Samaisukh Sophasan [b], Hitoshi Endou [c], Chuenchit Boonchird [a,*]

[a] *Department of Biotechnology, Faculty of Science, Mahidol University, Rama 6 Road, Phayathai, Rajathevee Bangkok 10400, Thailand*
[b] *Department of Physiology, Faculty of Science, Mahidol University, Rama 6 Road, Phayathai, Rajathevee Bangkok 10400, Thailand*
[c] *Department of Pharmacology and Toxicology, Kyorin University School of Medicine, 6-20-2 Shingawa, Mitaka, Tokyo 181-8611, Japan*

Received 11 April 2005; received in revised form 30 August 2005; accepted 27 September 2005
Available online 24 October 2005

Abstract

Organic anion transporter 1 (OAT1) is localized in the basolateral membrane of the proximal tubule in the kidney and plays an essential role in eliminating a wide range of organic anions, preventing their toxic effects on the body. Structural and functional studies of the transporter would be greatly assisted by inexpensive and rapid expression in the yeast *Saccharomyces cerevisiae*. The gene encoding rat OAT1 (rOAT1) contains many yeast non-preferred codons at the N-terminus and so was modified by fusion of the favored codon sequence of a hemagglutinin (HA) epitope preceding the start codon. The modified gene was cloned into several yeast expression plasmids, both integrative and multicopy, with either *ADH*1 promoter or *GAL*1 promoter in order to find a suitable expression system. Compared with the wild type gene, a substantial increase in rOAT1 expression was achieved by modification in the translational initiation region, suggesting that the codon chosen at the N-terminus influenced its expression. The highest inducible expression of rOAT1 was obtained under *GAL*1 promoter in 2 μ plasmid. A large fraction of rOAT1 was glycosylated in yeast, unaffected by growth temperature. The recombinant yeast expressing rOAT1 showed an increase in the uptake of p-aminohippurate (PAH) and this showed a positive correlation with rOAT1 expression level. Location of rOAT1 predominantly in the yeast plasma membrane confirmed correct processing. The importance of glycosylation for rOAT1 targeting was also shown. To our knowledge, this is the first successful functional expression of rOAT1 in the yeast *S. cerevisiae*.

Keywords: Organic anion transporter 1; Membrane protein; *Saccharomyces cerevisiae*; Heterologous gene expression

1. Introduction

Numerous endogenous and exogenous organic anions can have harmful effects on the body. These compounds are either transformed into less active metabolites or are excreted via transport processes by excretory organs such as the kidney, liver and intestine. In the kidney, for example, a multitude of organic anions of varied structure are efficiently eliminated by transport systems in the proximal tubule [1].

rOAT1 is an essential component of the renal secretion system that mediates sodium-independent uptake of anionic compounds across the basolateral membrane into the proximal tubule in exchange for intracellular glutarate. The substrate specificity of rOAT1 is remarkably wide [2] and a variety of drugs have also been demonstrated to be transported by it [3,4]. Efflux of these substances through the luminal membrane is presumed to occur via anion exchangers and/or electrochemical gradient-driven facilitated transporters [1,2,4,5].

So far, structural and functional studies of rOAT1 have been hampered by the lack of a sufficient amounts and heterologous expression in a functional form would be a possible way to solve this problem. Although rOAT1 has been functionally expressed in *Xenopus leavis* oocytes [6,7], manipulation of the test system is time consuming and the protein yield is often poor. The yeast *Saccharomyces cerevisiae* has been successfully used for expression of several mammalian membrane proteins such as cystic fibrosis transmembrane conductance regulator [8], human multidrug resistance [9], vesicular monoamine transporter [10], dopamine receptor [11], and glucose transporter [12] and could thus be considered as a possible vehicle for inexpensive and rapid production of rOAT1.

* Corresponding author. Tel.: +66 2201 5304; fax: +66 2354 7160.
E-mail address: scebc@mahidol.ac.th (C. Boonchird).

0005-2736/$ - see front matter © 2005 Elsevier B.V. All rights reserved.
doi:10.1016/j.bbamem.2005.09.021